

Changes in seismicity in a volcanically active region, on the eastern side of Izu Peninsula, Japan

K. Z. Nanjo,^{1,2,3,4*} Y. Yukutake⁵, T. Kumazawa³

¹Global Center for Asian and Regional Research, University of Shizuoka, 3-6-1 Takajo, Aoi-ku, Shizuoka 420-0839, Japan

²Center for Integrated Research and Education of Natural Hazards, Shizuoka University, 836 Oya, Suruga-ku, Shizuoka 422-8529, Japan

³Institute of Statistical Mathematics, 10-3 Midori-cho, Tachikawa, Tokyo 190-8562, Japan

⁴Japan Agency for Marine-Earth Science and Technology, Yokohama Institute for Earth Sciences, 3173-25 Showa-machi, Kanazawa-ku, Yokohama, Kanagawa 236-0001, Japan

⁵Earthquake Research Institute, The University of Tokyo, 1-1-1 Yayoi, Bunkyo-ku, Tokyo 113-0032, Japan

*Correspondence and requests for materials should be addressed to K.Z.N. (email: nanjo@u-shizuoka-ken.ac.jp)

ORCID: 0000-0003-2867-9185 (K. Z. N.); 0000-0002-1533-4885 (Y. Y.); 0000-0003-2435-640X (T. K.)

Highlights

- We study seismicity during 2005-2020 in a volcanic region of Izu Peninsula, Japan
- Result showed seismic quiescence with its starting point falling in period 2009-2013
- This result was common between ordinary earthquakes and low-frequency earthquakes
- Seismic quiescence occurred without a significant uplift during the studied period
- Magma source causing an uplift implies a transition phase to be an inactive state

Abstract

The Izu-Tobu region, on the eastern side of Izu Peninsula, in Japan, is volcanically and seismically active. In this region, earthquake swarms of ordinary earthquakes frequently occur at shallow depths, which is considered to be associated with magma intrusion. Beneath ordinary earthquakes, low-frequency earthquakes (LFEs) are infrequently observed. We conducted a timeseries analysis of both types of earthquakes during the time period 2005-2020, using a variant of the Epidemic-Type Aftershock Sequence model. For this analysis, we used the Japan Meteorological Agency catalog of ordinary earthquakes and the catalog of LFEs produced using the matched filter method. The observed result, which was common to both types of earthquakes, showed a significant change in seismicity, which became quiet, with the inflection point falling sometime between late 2009 and mid-2013, during which two out of three pronounced earthquake swarms occurred. We associated this seismic quiescence with changes in background rate to be low, where background rate, by removing the triggering effect of aftershocks, was interpreted as having been caused directly by the magma source, which can vary with time. We used surface displacement data obtained from the Geospatial Information Authority of Japan, and observed that the uplift due to magma intrusion was significant during the 1970s-1990s whereas it was in abatement or unobservable during the studied period (2005-2020). We also found that the seismic quiescence occurred without significant crustal movement during the studied period. Our implication from this finding is that magma source, which caused magma intrusion into the Izu-Tobu region, is in a transition phase, becoming less active, compared with the magma source during the 1970s-1990s. We pointed out that this implication is consistent with the history of repeated uplift events obtained from morphological and stratigraphic survey conducted in and around the Izu-Tobu region.

Keywords:

Volcano monitoring, Intra-plate processes, Seismicity and tectonics, Volcano seismology, Computational seismology, Asia

Abbreviations

AIC: Akaike Information Criterion

EMR: Entire-Magnitude-Range

ERC: Earthquake Research Committee

ERI: Earthquake Research Institute

ETAS: Epidemic-type Aftershock Sequence

GEONET: GNSS Earth Observation Network System

GNSS: Global Navigation Satellite System

GR: Gutenberg-Richter

GSI: Geospatial Information Authority of Japan

IBM: Izu-Bonin-Mariana

JMA: Japan Meteorological Agency

LFE: Low-frequency earthquake

MF: Matched-filter

MLE: Maximum-likelihood estimate

1. Introduction

The Izu Peninsula in central Japan is in the northern most part of the Izu Bonin Marian (IBM) Arc and is located in the collision zone with Honshu Island, where crustal deformation is active (Fig. 1). This Peninsula is volcanically and seismically active (Aramaki and Hamuno, 1977). The eastern side of the Izu Peninsula is a monogenic volcano field where volcanoes are included in the Izu-Tobu Volcano Group (Koyama and Umino, 1991). This Volcano Group is listed as an active volcano where the Japan Meteorological Agency (JMA) operates 24-hours monitoring in a real-time manner. In the 1920s-1930s and 1970s-1990s, earthquake swarms, which consist of seismicity that lacks an obvious mainshock-aftershock sequence, and crustal deformation actively occurred, associated with magmatic activities (Geospatial Information Authority of Japan, 2016; Shishikura et al., 2023), where the Geospatial Information Authority of Japan is hereinafter referred to as GSI. Ishida (1984) applied the volcanic model of Hill (1977) to interpret a 1980 earthquake swarm. Shimazaki (1988) suggested a dyke intrusion mechanism as a possible source of persistent swarms in the region east of the Izu Peninsula. Furthermore, associated with swarm activity in 1988, Tada and Hashimoto (1989) proposed a model of tensile fault to account for the horizontal and vertical displacement fields around the eastern Izu Peninsula.

In 1989, an eruption occurred off the east coast of the Izu Peninsula after the start of earthquake swarms, and then formed the Teishi Knoll (e.g., Yamamoto et al., 1991; Nagamune et al., 1992), one of the members of the Izu-Tobu Volcano Group. Geodetic and seismic data have been analyzed to explain the swarms on the basis of the dike intrusion process (Okada and Yamamoto, 1991; Okada et al., 2000; Hayashi and Morita, 2003; Morita et al., 2006; Miyamura et al., 2010). Okada and Yamamoto (1991) proposed a model consisting of two tensile faults corresponding to a series of magma intrusions, and a right-lateral reverse fault representing an earthquake of magnitude (M) 5.5,

corresponding to the largest event in this swarm. From their model, Okada and Yamamoto (1991) concluded that the intersection of the right-lateral reverse fault with one of the tensile faults caused magma to rise into soft sedimentary layers at the sea-bottom, creating a lava dome, i.e., the Teishi Knoll. Later, instability brought about a magma-phreatic explosion.

The swarm activity in 1998 was also accompanied by crustal deformation, and was well modelled by the dyke opening process (Okada et al. 2000). The swarm's hypocenters in 1998, which were precisely defined, were mainly aligned on a thin vertical plane (Hayashi and Morita, 2003; Morita et al., 2006). The normal direction to the plane coincided well with the direction of tectonic extensional stress around the hypocentral area (Ukawa, 1991). At the beginning of activity, a small fraction of the events occurred at a greater depth, where hypocenters aligned on a vertical line and migrated upward. After one day from the beginning, hypocenters reflected an expansion downward and upward of the dyke from the center of the swarm by excess magma pressure on the inside (Hayashi and Morita, 2003; Morita et al., 2006).

Miyamura et al. (2010) found that the duration of earthquake swarms in the Izu region was associated with the largest variation in the volumetric strain records at the Higashi-Izu JMA station within 24 hours from the early stages of the swarms. Consequently, in 2010 the Japan governmental Earthquake Research Committee (ERC) investigated the statistical relationships between the volumetric strain records and seismicity to forecast the magnitudes of swarm activities (ERC, 2010). Kumazawa et al. (2016) used the ETAS (Epidemic-Type Aftershock Sequence) model (Ogata, 1988) on eight swarms after mid-1980 to explore their relationship with the volumetric strain recorded by the Higashi-Izu station. They proposed that the ETAS model may be helpful in monitoring magma intrusions that drive the changes in stress.

While swarms occur at a depth range of <20 km (black symbols in Fig. 1), earthquakes during non-swarm periods also occur with the same depth range. These are high-frequency and ordinary earthquakes while low-frequency earthquakes (LFEs) occur at a depth range of 30-40 km (red symbols in Fig. 1). The characteristics of ordinary earthquakes (including not only swarm earthquakes but also non-swarm earthquakes) and LFEs are still uncertain. The primary purpose of this study was to examine whether the ETAS model is applicable to both types of earthquakes as a first step to clarify their characteristics. Knowing this might allow us to better understand whether magma source can vary with time. Our study region, which included the main seismic activity in 2005-2020 is indicated by a black rectangle shown in Figs. 1b and 2b, and referred in this paper as the Izu-Tobu region, where the LFEs are located almost immediately below ordinary earthquakes

(Fig. 1).

Using the earthquake catalog maintained by JMA, more than 10,000 ordinary earthquakes occurred during 2005-2020, and there were swarms in 2006, 2009 and 2011 (Fig. 2). On the other hand, LFEs were observed 47 times during the same period. JMA, which employed conventional event-detection methods, might have had difficulty in detecting LFEs that are easily buried in noise due to their low signal-to-noise ratios. To resolve this difficulty, we produced a LFE catalog using the matched-filter (MF) method, which cross-correlated a template to continuous seismic signals (Yukutake, 2017; Yukutake et al., 2019). Our resultant catalog included 895 LFEs during the period 2005-2020. This is about 19 times more than the number of earthquakes (47) reported by JMA during the same period. This means that LFEs occurred more frequently than were previously thought.

We conducted the ETAS analysis of ordinary earthquakes and LFEs to detect changes in seismicity rate for both types of earthquakes. We showed that changes in seismicity rate became low (called seismic quiescence) for both types of earthquakes during the analyzed period (2005-2020). Our result coincides with the geodetic observation that indicates that uplift was in abatement and unobservable in the 2000s and later.

2. Data

2.1. Ordinary earthquakes, LFEs, and the study region

The JMA catalog includes ordinary earthquakes and LFEs in Japan. Although ordinary earthquakes are distributed all over Japan, LFEs tend to concentrate beneath active volcanoes, along the boundary between the Philippine Sea Plate and the continental plate in western Japan (Obara, 2002), and as several isolated clusters in the intraplate regions (Aso et al., 2013). Each event in the JMA catalog is classified based on subsidiary information: natural (ordinary) earthquake, LFE, artificial event, etc.

Ordinary earthquakes in the Izu-Tobu region during 2005-2020 show that the three seismic swarms started in 2006, 2009, and 2011 (Fig. 2) and their the respective periods of main activities were Mar. 1-Apr. 30, 2006, Dec. 17-21, 2009, and Jul. 17-18, 2011 (GSI, 2016). Locations of these swarms overlapped or were close to each other. Their depths ranged from 0 to 20 km (Fig. 1c). This is consistent with a previous swarm that started in 1989 (Hayashi and Morita, 2003; Morita et al., 2006). LFEs in the Izu-Tobu region were separated from those in other regions (Fig. 1a). LFEs occurred at depth of 30-40 km beneath ordinary earthquakes (Fig. 1). We defined the box (139.02-139.23°E, 34.87-35.0°N, and depth of 0-40 km) as the study region called the Izu-Tobu

region (Figs. 1a and 2b). The region includes LFEs and the main activities of the three swarms of ordinary earthquakes.

The number of ordinary earthquakes with $M \geq -1$ within the study region in 2005-2020 is more than 10,000, while the number of LFEs with $M \geq -1$ is 47. We used these ordinary earthquakes in the JMA catalog for further analysis. On the other hand, given that the number of LFEs is small, we thought that the characteristics of LFEs could not be fully understood. Given that LFEs in the Izu-Tobu region were deeper than ordinary earthquakes, and due to the low signal-to-noise ratios of LFEs, it is likely difficult to detect LFEs with conventional event-detection methods employed by JMA.

2.2. The MF method

To resolve the difficulty in detecting LFEs by conventional event-detection methods, we produced a catalog of LFEs using the MF method (Peng and Zhao 2009; Shelly et al., 2007; Kato et al., 2012; Yukutake, 2017; Ross et al., 2019; Yukutake et al., 2019). In this method, which considers a continuum of seismic signals, an LFE is identified when the timing of a seismic signal and the timing of a template signal overlap. In this study, the MF system used for detecting LFEs beneath the Hakone volcano, Japan (Yukutake, 2017; Yukutake et al., 2019) was modified so that it was applicable to the Izu-Tobu region.

Waveforms of continuous signals that were used in this study covered the Jan. 2005-Dec. 2020 period, as recorded by 20 seismic stations (Fig. 3a) with a three-component velocity seismometer in and around the Izu-Tobu region. These data were obtained from the Earthquake Research Institute (ERI) at the University of Tokyo.

To prepare template LFEs, we used the JMA catalog to select events classified as LFEs in the Izu-Tobu region. This study relied on statistical analyses of the LFE catalog covering the studied time interval. It should be noted that the catalog may be controlled by the selection of template earthquakes in the MF analysis. Large LFEs with $M \geq 0.2$ were selected in order to allow template waveforms to include more information on signals than on noise. Then, among them, LFEs that were recorded by six stations with a minimum signal-to-noise-ratio of 2, were selected (Yukutake et al., 2019).

The MF procedure to identify LFEs, briefly described in this paragraph, is the same as that of Yukutake et al. (2019) (also see Yukutake, 2017). Three-component waveform records for each template LFE were used, applying a six-second time window beginning two seconds before the onset time of the theoretical S-wave arrivals. Both templates and continuous waveforms were bandpass-filtered for 1-6 Hz and decimated at 20 Hz to reduce the calculation cost. This band was

selected according to Yukutake (2017) and Yukutake et al. (2019), although other studies used a slightly narrower band such as 1-4 Hz by Kurihara and Obara (2021). The correlation coefficients (CC) between a template and continuous waveform at each sampling time for every component at each station were calculated. After subtracting the hypocenter-to-station travel time of the theoretical S-wave, the time sequences of the correlation function throughout all channels were stacked. When the peak of the stacked correlation function exceeded a threshold level of nine times the median absolute deviation, an event was identified as a candidate LFE. After removing multiple counts, the location of the candidate was assigned to the hypocenter of the matched template LFE determined by JMA. Magnitude was determined as the mean of the maximum amplitude ratios of the template with respect to the candidate. The MF procedure described above was applied to all waveform records in the time period Jan. 2005-Dec. 2020, and a preliminary catalog, including candidate LFEs, was created, although LFEs identified by five or less stations were not included in this catalog (Yukutake, 2017; Yukutake et al., 2019).

2.3. Finalized catalog of LFEs

Less reliable LFEs were removed from the preliminary catalog to create a finalized catalog, as follows. Among candidate LFEs, false detection occasionally occurred due to contamination by other seismic signals such as teleseismic earthquakes. This contamination led to the detection of LFEs with a large M , so we visually inspected whether each template LFE was used to detect many candidate LFEs with $M > 1.5$, a magnitude above which LFEs have never been recorded by JMA in the Izu-Tobu region since 2005. We considered that such template LFEs had a feature similar to teleseismic earthquakes and decided to eliminate them from the list of template LFEs. Thus, candidate LFEs detected by using the eliminated template LFEs were removed from the preliminary catalog, resulting in the finalized catalog that included about 2502 LFEs. Despite this quality test, an additional test was conducted, as described in the next paragraphs.

The CC -values of LFEs in the intermediate catalog (Fig. 3b) ranged between 0.1 (poor correlation with a template LFE) and 1 (strong correlation with, and identical to, the corresponding template LFE). Setting the minimum CC to a low value implies the use of an incomplete catalog influenced by the nature of low signal-to-noise ratios of LFEs. The minimum threshold for CC (CC_{th}), above which LFEs were used for our analysis, should be above the upper noise limit. Histograms of CC -values in Fig. 3b show an asymmetric distribution with a tall peak at $CC \sim 0.15$. We followed previous studies (Green and Neuberg, 2006; Petersen 2007; Lamb et al. 2015), in which the distribution of lower CC -values was modeled by a normally distributed curve that would be

expected for random correlations between signals and noise, while the upper tail was considered to represent the presence of well-correlated LFEs. Visual inspection shows that frequencies at and below $CC \sim 0.15$ are in good agreement with the left-hand side of the normally distributed curve where the mean is 0.155 and its standard deviation is 0.02 (Fig. 3b). We selected $CC_{th}=0.25$, which is larger than the mean plus three standard deviations. The histogram for $M \geq 0$ is also displayed because our analysis basically did not include LFEs with $M < 0$. A total of 35 template LFEs were used for the intermediate catalog.

The scope of this study did not permit us to reveal repeating LFEs, nor cyclic activities and cluster characteristic, as were studied by Lamb et al. (2015). Rather, this study's objective was to resolve the difficulty in detecting smaller LFEs. Our future research will conduct in-depth analyses of repeating LFEs for each cluster in the Izu-Tobu region, referring to Lamb et al. (2015), and using a sophisticated MF method that can locate detected LFEs to appreciate whether they occurred in the same cluster as the template LFE used to find them.

The number of LFEs (894) in our finalized catalog of $CC_{th}=0.25$ (Fig. 3c) is about 19 times larger than in the JMA catalog, which lists 47 LFEs detected in 2005-2020 by a conventional method that is not based on CC .

3. Methods

3.1. ETAS model and change point analysis

The ETAS model (Ogata, 1988) was originally introduced for ordinary earthquakes, but we assumed that the model can be extended and applied for both ordinary earthquakes and LFEs in the Izu-Tobu region. In this section, when the word "earthquake" is used, the reader should understand that it includes both ordinary earthquakes and LFEs.

The ETAS model is a point-process model that represents the activity of earthquakes of a minimum magnitude (M_{th}) and above in a certain region during a specified time interval. Seismic activity includes the background activity at a constant occurrence rate μ (Poisson process). The model assumes that each earthquake (including the aftershock of another earthquake) is followed by aftershocks. Aftershock activity is represented by the Omori-Utsu formula (Utsu, 1961) in the time domain. The rate of an aftershock occurrence at time t following the i -th earthquake (time t_i and magnitude M_i) is given by $v_i(t) = K_0 \exp\{\alpha(M_i - M_{th})\} (t - t_i + c)^{-p}$ for $t > t_i$, where K_0 , α , c , and p are constants, which are common to each target aftershock sequence in a region. The rate of occurrence of the whole earthquake series at t becomes $\lambda(t|H_t) = \mu + \sum_{S < t_i < t} v_i(t)$. The summation is performed for all i satisfying $t_i < t$. Here, H_t represents the history of occurrence times with associated

magnitudes from the data $\{(t_i, M_i)\}$ before time t . The parameter set $\theta=(\mu, K_0, \alpha, c, p)$ represents the characteristics of seismic activity. The units of the parameters are day^{-1} , day^{-1} , no unit, day, and no unit, respectively. For the case of $K_0=0$, the ETAS model reduces to the Poisson model. We estimated these parameters using the maximum-likelihood estimate (MLE). Because K_0 differs depending on reference magnitude M_z (Ogata, 2006), we followed Ogata (2006) and implemented the largest magnitude as the reference magnitude: namely, we implemented $M_z=1.5$ for LFEs and $M_z=5.8$ for ordinary earthquakes throughout this study.

Using the MLE, it is possible to visualize how well or poorly the model fits an earthquake sequence by comparing the cumulative number of earthquakes with the rate calculated by the model. If the model presents a good approximation of observed seismicity, an overlap with each other is expected.

A FORTRAN program package (SASeis2006) associated with a manual for the ETAS analysis was used to calculate MLEs and also to visualize model performance (Ogata, 2006). This was extended to the program package XETAS (Ogata and Tsuruoka, 2016) using a graphical user interface.

When the stationary ETAS model does not fit a dataset well, the simplest alternative model is a two-stage ETAS model (e.g., Kumazawa et al., 2010, 2017, 2019; Nanjo et al., 2023) that considers different parameter values in subperiods before and after a particular time, referred to as change-point T_c . The Akaike Information Criterion (AIC) is used to test whether or not the changes in seismicity pattern at T_c is statistically significant (Akaike, 1974). In this procedure, we separately fitted the ETAS models for each divided period and then compared their total goodness-of-fit values against the one-fit value over the whole period using the principle of minimum AIC. AIC was calculated from the maximum log-likelihood and number of adjusted parameters.

If T_c is hypothetically prefixed based on some information other than the occurrence data, such as a notable geophysical event or a notable outside large earthquake, $\text{AIC}_{\text{single}}$ (AIC for the model fitted over the whole period) can be compared with $\text{AIC}_{2\text{stage}}$ (AIC for the 2-stage model fitted on divided periods) to select the model with the smaller value that performs a better fit to the data in the entire target period. Here, $\text{AIC}_{2\text{stage}}=\text{AIC}_1+\text{AIC}_2$ (AIC_1 and AIC_2 for fitting to the 1st and 2nd subperiods, respectively). If T_c is searched from the target data, the 2-stage model becomes harder to accept. Namely, $\text{AIC}_{2\text{stage}}$ plus the penalty term $2q$ is compared with $\text{AIC}_{\text{single}}$ to select the model. Here q is the degree of freedom to search for the best candidate T_c from the data. q depends on sample size (number of earthquakes in the target period) (Ogata, 1992; Kumazawa et al., 2010), and increases with sample size.

One may also be interested in the error range of T_c (e.g., Kumazawa et al., 2010). Although the standard theory for the MLE error is not applicable to the change-point problem, confidence intervals in terms of the AIC differences can be provided as noted below. We considered the likelihood of the models with different change-point candidates T_0 in terms of AIC (e.g., Akaike, 1978a, 1978b), given by $\exp[-\{AIC_{2stage}(T_0)+2q\}/2]$. The normalization of these likelihoods regarding all T_0 values assigns a probability mass around the MLE, providing error bounds. Unlike the ordinary MLE, the likelihood can be multimodal, which provides longer error bars. In this study, we provided a 68% confidence interval.

3.3. Choice of M_{th}

Analyses of the ETAS model of LFEs during a specified time interval are critically dependent on the choice of the M_{th} value. To select it, we referred to estimates of completeness magnitude (M_c) of the processed data of LFEs. Above M_c , all LFEs are considered to be detected. A too-low value of M_{th} , compared to estimates of M_c , leads to an unreliable ETAS fitting. Details of M_c are provided in the “Computation of M_c ” section.

M_c for LFEs was about 0.2~0.4, based on pre-catalogs covering three time periods: 2005-2009, 2010-2014, and 2015-2020 (Fig. 4). We chose $M_{th}=0.3$ ($M \geq 0.3$) for analyses of the ETAS model of LFEs. We also considered $M_{th}=0.4$ ($M \geq 0.4$) to suggest a generally stable feature.

Similar to the LFEs, we estimated M_c values for ordinary earthquakes. A single value of M_c over the entire catalog was not considered, but timeseries of M_c , obtained from taking a moving window approach, was considered, where the window covered 100 ordinary earthquakes. The reason for adopting this moving window approach was to calculate the local properties of an input data stream and an output M_c variation. M_c values were generally about 1, except for the timings of the swarms in 2006 and 2009 where M_c values were above 1 (Fig. 4). We chose $M_{th}=1$ ($M \geq 1$) for analyses of the ETAS model of ordinary earthquakes. We also considered another value ($M_{th}=1.5$) for the same reason as that described for LFEs.

3.4. Computation of M_c

To compute M_c for a given time interval, we used the Gutenberg-Richter (GR) relation (Gutenberg and Richter, 1944), given by $\log_{10}N=a-bM$, where N is the number of earthquakes with a magnitude larger than or equal to M in the given time window, and a and b are constants. b is used to describe the relative occurrence of large and small events in the given time window (i.e., a high b -value indicates a larger proportion of small earthquakes, and vice versa). We assumed that the GR relation

was applicable to ordinary earthquakes and LFEs (e.g., Wiemer, 2001; Schorlemmer et al., 2003; Woessner and Wiemer, 2005; Nanjo and Yoshida, 2018; Nanjo, 2020; Nanjo et al., 2023). In this section, the word “earthquake” includes both ordinary earthquakes and LFEs.

We employed the Entire-Magnitude-Range (EMR) technique (Woessner and Wiemer, 2005), which simultaneously calculates the a -, b - and M_c -values. Among existing techniques, the EMR method shows superior performance when applied to synthetic test cases or real data from regional and global catalogs (Woessner and Wiemer, 2005). The software package ZMAP (Wiemer, 2001) was used to facilitate the computation of a , b , and M_c based on the EMR method. Fig. 4a shows a good fit of the GR relation to observations in the present cases. We also used a tool facilitated in ZMAP to compute uncertainty in b and M_c based on a bootstrapping technique (Schorlemmer et al., 2003).

4. Results

4.1. First-order timeseries analysis

We conducted a first-order timeseries analysis using the ETAS model, based on the entire period Jan. 2005-Dec. 2020. We compared AIC for a single (standard) ETAS fitting, AIC_{single} , with AIC for a two-stage ETAS fitting, AIC_{2stage} , to select the model with the smaller value. ΔAIC ($=AIC_{\text{single}}-AIC_{\text{2stage}}$) of ordinary earthquakes with $M \geq 1$, as a function of T_c (blue data in Fig. 5a), shows that the two-stage ETAS model was much better than the single ETAS model during $T_c=480-4050$ days. In this range of T_c , where ΔAIC was above the horizontal dashed line in blue, which represents a hurdle to the selection of the two-stage ETAS model, we observed three pronounced peaks in ΔAIC at the timings of the three swarms. The change point’s confidence interval of 68% (horizontal solid bars in blue) indicates that the most significant T_c -values were in 1820-2420 days (interval from late 2009 to mid-2011), during which the 2009 and 2011 swarms occurred (vertical blue and orange lines). A similar feature was observed for $M \geq 1.5$ (red data in Fig. 5a). The same analysis was conducted for LFEs (Fig. 5b). The most significant T_c -values were in 2730-3090 days for $M \geq 0.3$ and 2550-3080 days for $M \geq 0.4$. This indicates that a change point’s confidence interval was likely from late 2011 to mid-2013 or after the 2011 swarm (vertical orange line). A comparison between the two types of earthquakes shows that the most significant T_c -values for ordinary earthquakes were earlier than those for LFEs.

When ordinary earthquakes with $M \geq 1$ until $T_c=1820$ days (one of the most significant T_c -values) was fitted by ETAS, the occurrence rates (black) were smaller than the extrapolated rates (red) after $T_c=1820$ days (Fig. 6a). This indicates the relative quiescence of seismic activity. LFEs with $M \geq 0.3$

until $T_c=2740$ days (one of the most significant T_c -values) fitted by ETAS shows relative quiescence (Fig. 6b), a similar feature to ordinary earthquakes (Fig. 6a).

The above result is not induced by inclusion of a period around the timing of the first swarm in 2006 into the studied period (Jan. 2005-Dec. 2020). Namely, we examined whether seismic quiescence starting around the timings of the second and third swarms in 2009 and 2011 appeared to remain stable without a period around the timing of the first swarm in 2006 (Fig. 7). To examine this, we conducted an ETAS analysis of ordinary earthquakes and LFEs during the subperiod Jan. 2008-Dec. 2020. Results show that the general $\Delta\text{AIC}-T_c$ patterns (Fig. 7) for both types of earthquakes were similar to those during the corresponding period in Fig. 5. The change point's confidence interval coincided with the timing of the 2009 swarm for ordinary earthquakes, but it emerged after the 2011 swarm for LFEs. Similar to the analysis for the entire period (Fig. 5), the most significant T_c -values for ordinary earthquakes were earlier than those for LFEs.

4.3. Second-order timeseries analysis

We conducted a second-order timeseries analysis using the ETAS model, based on the subperiods Jan. 2005-Dec. 2008 for ordinary earthquakes and Jan. 2005-Dec. 2010 for LFEs (Fig. 8). We considered these subperiods, including a pronounced peak in ΔAIC before the change point's confidence intervals seen in the results for the entire period, namely the confidence interval from late 2009 to mid-2011 for ordinary earthquakes (Fig. 5a) and the confidence interval from late 2011 to mid-2013 for LFEs (Fig. 5b). The results of ordinary earthquakes with $M_{\text{th}}=1$ and 1.5 in Fig. 8a show that the change points' confidence intervals were limited to the timing of the 2006 swarm (vertical yellow bar). In contrast, the results of LFEs with $M_{\text{th}}=0.3$ and 0.4 in Fig. 8b show that the confidence intervals were not limited to it. Rather, the confidence intervals for LFEs were after the timing of the 2006 swarm. ΔAIC for LFEs with $M_{\text{th}}=0.4$ (red data in Fig. 8b) showed a better but insignificant outcome when the two-stage ETAS model, rather than the single ETAS model, was used. Namely, ΔAIC was higher than 0 ($\Delta\text{AIC}>0$), but it was below the horizontal dashed line, which is a hurdle to the selection of the two-stage ETAS model. We interpreted this insignificant outcome as an indication that the number of LFEs with $M\geq 0.4$ was not enough to achieve the desired conclusion. Visual inspection of T_c for ΔAIC , indicated by green circles in Fig. 8, shows relative quiescence of both types of earthquakes (Fig. 9).

Overall, the first-order observation is that seismic quiescence for both types of earthquakes started during the period from late 2009 to mid-2013 when the 2009 and 2011 swarms occurred. The start of seismic quiescence was earlier for ordinary earthquakes than for LFEs. Beyond that, we concluded

that the second-order seismic quiescence occurred before the start of the first-order seismic quiescence. The second-order seismic quiescence started around the timing of the 2006 swarm. A second-order timeseries analysis showed the earlier start of seismic quiescence for ordinary earthquakes than for LFEs, a similar feature to the first-order timeseries analysis.

4.4. Background rate

A challenge in exploring the reason for the changes in the occurrence rate (seismic quiescence) of the two types of earthquakes (Figs. 5-9) is that the magma source, which is underground and directly unobservable, results in heterogeneous occurrence times of both earthquakes. To tackle this problem, we took a reductionism approach, decomposing all earthquakes into primary earthquakes and secondary-triggered earthquakes. Measuring the occurrence rate of the former primary earthquakes (indicative of Poisson background activity), separated by the latter secondary-triggered earthquakes (indicative of aftershock activity), allows the magma source to be inferred (Kumazawa et al., 2016). In this context, the term “background rate” means the occurrence rate of a primary earthquake that is directly caused by either tectonic or magma sources that can vary with time (Kumazawa et al., 2016). Past studies (Hainzl and Ogata, 2005; Llenos et al., 2009; Llenos and McGuire, 2011; Brodsky and Lajoie, 2013) indicated that variation in stress affect the background rate.

Although a sophisticated nonstationary model is available (e.g., Kumazawa and Ogata, 2013; Kumazawa et al., 2017), a simple approach was adopted to capture essential aspects of the time-dependent background activities. This involves taking a time-window approach. We considered the results obtained from the first-order timeseries analysis (Jan. 2005-Dec. 2020), and compared the background rate (μ) between the periods before and after the T_c -value for ΔAIC , as indicated by the green circle in Fig. 5. The results of ordinary earthquakes (Fig. 6a) showed that $\mu=0.019$ for the period before $T_c=1820$ days was larger than $\mu=0.003$ after it. Similarly, the results of LFEs (Fig. 6b) showed a larger μ -value for the period before $T_c=2740$ days ($\mu=0.046$) (Fig. 6b) than for the period after it ($\mu=0.022$). We adopted the same comparison in μ for the second-order timeseries analysis of ordinary earthquakes (Jan. 2005-Dec. 2008) and LFEs (Jan. 2005-Dec. 2010). The results of $\mu=0.024$ before $T_c=480$ days and $\mu=0.010$ after it for ordinary earthquakes (Fig. 9a) and $\mu=0.069$ before $T_c=620$ days and $\mu=0.029$ after it for LFEs (Fig. 9b) showed a similar feature to that for the first-order timeseries analysis.

We associated the seismic quiescence observed in the first- and second-order timeseries analysis with a decrease in μ . Similar to previous studies (Hainzl and Ogata, 2005; Llenos et al., 2009; Llenos and McGuire, 2011; Brodsky and Lajoie, 2013; Kumazawa et al., 2016), the changes in μ

were attributed to variation in stress caused by the magma source.

5. Discussion and conclusions

We considered crustal movement data from a leveling survey by GSI and station coordinates derived from the Global Navigation Satellite System (GNSS) maintained by GSI to show that seismicity became quiet when there was no significant uplift in the Izu-Tobu region.

A leveling survey along the eastern coast of the Izu Peninsula since 1904 until 2015 (Fig. 10) showed a secular variation of the four benchmarks (9335, 9336, 9337, 9338) referred to as benchmark 9328 (GSI, 2016). The former four benchmarks were located in the Izu-Tobu region while the latter reference benchmark was located outside of the northern periphery of this region. The upward and downward crustal movement of the four benchmarks relative to the reference benchmark is interpreted as an indication of uplift and subsidence of the Izu-Tobu region, respectively. A brief summary of crustal movement in the Izu-Tobu region is given as follows. The uplift progressed during the 1920s-1930s, where the 1923 *M*7.9 Kanto earthquake and the 1930 *M*7.3 Kita Izu earthquake occurred outside the Izu-Tobu region, while the 1930 swarm occurred inside the region. Until the early 1970s, pronounced crustal movement was not observed. Around the timing of the 1974 Izu Hanto-oki earthquake, the uplift started to make noticeably progress. It continued until the late 1990s, after which the uplift was in abatement. After the 2009 swarm ended, the uplift was not observed.

Graphs of relative height of the four stations, numbered 1, 2, 3, and 4 in the reference station ODAWARA in Fig. 11a and the reference station HATSUSHIMA in Fig. 11b, show that the no uplift was observed even after 2015, which is the last year of the leveling survey shown in Fig. 10. We selected the four stations and the two reference stations to consider the baselines, because we tried to mimic the configuration of the benchmarks used for the leveling survey (inset of Fig. 10). To create Fig. 11, we used station coordinates derived from the GNSS Earth Observation Network System (GEONET) (Muramatsu et al., 2021; Takamatsu et al., 2023). The product in the current GEONET analysis strategy is called the F5 solution while that in the previous strategy is called the F3 solution. Blue and red data in Fig. 11 were based on the F5 and F3 solutions, respectively. The F5 solution was used for the period Oct. 2013-Dec. 2020, because data in the most recent 10-year period were obtained (see Data availability). To complement data since Jan. 2005 (start of our study period), the F3 solution was used for the period Jan. 2005-May 2016. Note that the periods for which the F3 and F5 solutions were used overlapped, covering the same period Oct. 2013-May 2016, providing justification for the consistency between these solutions (Fig. 11). Similarly, Fig. 12 was created for

the reference station YUGAWARA-A, which was in operation since the end of Mar. 2017.

For all the baselines, fluctuations in relative height were observed, and some of them were associated with antenna replacement of stations (triangle) and tree trimming around stations (arrow). We also observed an increase in the order of a few centimeters in relative height around the timing of the 2006 swarm in panel 4 of Fig. 11 (baselines ITOUYAHATANO-ODAWARA and ITOUYAHATANO-HATSUSHIMA), as seen in the leveling survey for benchmark 9338 (red curve in Fig. 10). However, the tendency that relative heights remained unchanged over time (no increasing nor decreasing trend in relative height) for all the baselines was generally observed. Combining the results of the leveling survey (Fig. 10) and those of baseline changes (Figs. 11 and 12) revealed no significant uplift in the studied period (Jan. 2005-Dec. 2020).

In volcanic or geothermal regions, earthquake swarms are common phenomena. These have been attributed to stress perturbations by magma intrusions (Einarsson and Brandsdottir, 1980; Dieterich et al., 2000; Okada et al., 2000; Toda et al., 2002; Waite and Smith, 2002; Feuillet et al., 2004; Smith et al., 2004) or fluid injections (Hainzl and Ogata, 2005; Lei et al., 2008; Terakawa et al., 2013; Terakawa, 2014). On the other hand, they can also be triggered by creep or slow-slip events (Ozawa et al., 2003; Delahaye et al., 2009; Segall et al., 2006). Thus, a swarm is thought to be driven by aseismic events that temporarily modify the stress state within the crust.

Kumazawa et al. (2016) used the ETAS model (Ogata, 1988) of eight swarms of ordinary earthquakes after mid-1980 to associate μ with volumetric strain recorded by the strainmeter located at the Higashi-Izu JMA station (139.0508°E, 34.8025°N), at the southern end of the Izu-Tobu region. Given that the pattern of strain variation at this station depends on magma intrusion (ERC, 2010), they proposed that the ETAS model may help in monitoring magma intrusions that drive the stress changes. In the Izu-Tobu region, some ordinary earthquakes consist of swarms whereas others are non-swarm ordinary earthquakes. Moreover, below ordinary earthquakes, LFEs occur (Fig. 1).

We conducted a timeseries analysis of the two types of earthquakes during Jan. 2005-Dec. 2020, using the standard single ETAS model and an alternative two-stage ETAS model considering different parameter values in subperiods before and after T_c . Our primary result supported successful modeling of the two types of earthquakes using the ETAS models. Detailed results are summarized next. The latter two-stage model was significantly better than the former single model, when the T_c -value fell in the period between late 2009 and mid-2013, when the 2009 and 2011 swarms occurred (Fig. 5). The seismicity rate before this T_c -value was larger than that after it (Fig. 6), indicating that seismic quiescence started around the T_c -value. We associated this seismic quiescence with a change in μ , and interpreted it to be directly caused by the magma source, which can vary

with time. These results were common to shallow ordinary earthquakes and deep LFEs.

We obtained similar results, conducting the same timeseries analysis during subperiods in which only the 2006 swarm was included (Figs. 8 and 9), using short catalogs: Jan. 2005-Dec. 2008 for ordinary earthquakes and Jan. 2005-Dec. 2010 for LFEs. Results showed that seismic quiescence started at T_c around the timing of the 2006 swarm.

For a comparison with subsurface seismicity in the Izu-Tobu region, surface vertical displacement data obtained from a leveling survey and the GEONET were used (Figs. 10-12). We observed that the uplift due to magma intrusion was significant during the 1970s-1990s while it was in abatement or unobservable in the 2000s and later. Thus, we found that the seismic quiescence observed in Figs. 5-9 occurred with no significant crustal movement during the studied period (Jan. 2005-Dec. 2020) in the Izu-Tobu region. Our finding based on seismicity and crustal deformation can be explained by the fact that the magma source, which transported magma that intruded into the Izu-Tobu region, was in a transition phase becoming inactive, after having been active during the 1970s-1990s.

Our observation is not the only or first evidence to indicate changes in seismicity without detectable crustal deformation at an active volcano area. A study on the active volcano Mt. Fuji (Nanjo et al., 2023) showed how LFEs in the deep part of the volcano revealed unrecognized activation after the Mar. 15, 2011 $M5.9$ Shizuoka earthquake at the foot of the volcano. Their analyses also showed that seismicity rate and μ of LFEs did not return to pre-earthquake levels, indicating a change in the magma system. No deformation of the crust around the volcano was reported during the $M5.9$ event.

The history of uplifts, obtained from a study based on morphology, stratigraphy, and fossil assemblages in the eastern side of the Izu Peninsula, revealed three events during 1500 years, each with an about 1-m uplift: a 1.05-m uplift in 595-715, a 1.33-m uplift in 1356-1666, and a 0.82-m uplift after 1830 (Shishikura et al., 2023). The repeated uplift events were caused by the activity of a monogenic volcano field or related seismo-tectonic processes (Shishikura et al., 2023). The cumulative uplift of 0.6-0.9 m since 1904, shown in Fig. 10, plus an uplift of about 0.1-0.2 m in 1868 or 1870 (Koyama, 1999) before the start of instrument measurement, roughly coincided with the most recent uplift of 0.82 m after 1830 (Shishikura et al., 2023). Given that the most recent uplift (0.82 m or 0.6-0.9 plus 0.1-0.2 m) is comparative to the two previous uplifts, the most recent uplift is thought to be in the final stage. Thus, our implication that magma source was in a transition phase becoming inactive is not surprising, and is consistent with the history of uplift events (Shishikura et al., 2023).

A question regarding our finding of the changes in seismicity rate was that the T_c -value for

shallow ordinary earthquakes was earlier than that for deep LFEs. Namely, the timing of the T_c -value for both types of earthquakes remains unexplained. Being able to answer this question would allow us to move toward a better understanding of how magma source changes with time as well as offering a better prediction regarding whether the seismicity continues quietly or is activated with/without the occurrence of a swarm. Our future work will be directed at answering this question.

Data availability

The datasets used and/or analyzed during the current study are available from the corresponding author upon reasonable request. The JMA catalog was obtained from <https://www.data.jma.go.jp/eqev/data/bulletin/hypo.html>. The waveform records were obtained from the permanent stations of the National Research Institute for Earth Science and Disaster Resilience, ERI at the University of Tokyo, JMA, and the Hot Springs Research Institute of the Kanagawa Prefectural Government. The location of Teishi Knoll, used for Figs. 1 and 2, was obtained from <https://www.mri-jma.go.jp/Dep/sei/fhirose/plate/en.PlateData.html>. The seismicity analysis software ZMAP (Wiemer, 2001), used for Fig. 4, was obtained from <http://www.seismo.ethz.ch/en/research-and-teaching/products-software/software/ZMAP>. The program XETAS (Ogata and Tsuruoka, 2016), used for Figs. 5-9, was obtained from <http://evrssl.eri.u-tokyo.ac.jp/software/xetas/index.html>. Data shown in Fig. 10 was reproduced from GSI (2016). Generic Mapping Tools (GMT) (Wessel et al., 2013), used for Figs. 1-3 and 10-12, is an open-source collection (<https://www.generic-mapping-tools.org>). GEONET data (Muramatsu et al., 2021; Takamatsu et al., 2023), used for Figs. 11 and 12, were obtained from <https://mekira.gsi.go.jp/index.en.html>.

CRedit authorship contribution statement

K. Z. Nanjo: Conceptualization, Investigation, Project administration, Formal analysis, Methodology, Software, Validation, Writing-original draft, Writing-review & editing. **Y. Yukutake:** Conceptualization, Investigation, Data curation, Resources, Writing-review & editing. **T. Kumazawa:** Investigation, Methodology, Software, Writing-review & editing.

Declaration of Competing Interests

The authors declare that they have no known competing financial interests or personal relationships that could have appeared to influence the work reported in this paper.

Data availability

Data, correspondence, and requests for materials can be addressed to K.Z.N.

Acknowledgments

We used the waveform records obtained from the permanent stations of the National Research Institute for Earth Science and Disaster Resilience, ERI at the University of Tokyo, JMA, and the Hot Springs Research Institute of the Kanagawa Prefectural Government. We also used the JMA earthquake catalog. This study was partially supported by the Ministry of Education, Culture, Sports, Science and Technology (MEXT) of Japan, under The Second Earthquake and Volcano Hazards Observation and Research Program (Earthquake and Volcano Hazard Reduction Research) (K.Z.N., Y.Y.) and under STAR-E (Seismology TowARD Research innovation with data of Earthquake) Program Grant Number JPJ010217 (K.Z.N., T.K.), JSPS KAKENHI Grant Numbers JP 22K03752 (Y.Y.), 20K11704 (T.K.), and a Research Grant of the Izu Peninsula UNESCO Global Geopark (K.Z.N., Y.Y.). The authors thank Y. Noda for help with implementing the MF method.

References

- Akaike, H., 1974. A new look at the statistical model identification. *IEEE Transactions on Automatic Control* 19(6), 716-723. <https://doi.org/10.1109/TAC.1974.1100705>.
- Akaike, H., 1978a. A Bayesian analysis of the minimum AIC procedure. *Annals of the Institute of Statistical Mathematics* 30, 9-14. <https://doi.org/10.1007/BF02480194>.
- Akaike, H., 1978b. On the likelihood of a time series model. *Journal of the Royal Statistical Society. Series D* 27, 217-235, <https://doi.org/10.2307/2988185>.
- Aso, N., Ohta, K., Ide, S., 2013. Tectonic, volcanic, and semi-volcanic deep low-frequency earthquakes in western Japan. *Tectonophysics* 600, 27-40. <https://doi.org/10.1016/j.tecto.2012.12.015>.
- Aramaki, S., Hamuro, K., 1977. Geology of the Higashi-Izu monogenetic volcano group. *Bulletin of the Earthquake Research Institute, University of Tokyo* 52, 235-278 (in Japanese with English abstract). <https://doi.org/10.15083/0000033207>.
- Brodsky, E.E., Lajoie, L.J., 2013. Anthropogenic seismicity rates and operational parameters at the Salton Sea geothermal field. *Science* 341(6145), 543-546. <https://doi.org/10.1126/science.1239213>.

- Delahaye, E.J., Townend, J., Reyners, M.E., Rogers, G., 2009. Microseismicity but no tremor accompanying slow slip in the Hikurangi subduction zone, New Zealand. *Earth and Planetary Science Letters* 277(1-2), 21-28. <https://doi.org/10.1016/j.epsl.2008.09.038>.
- Dieterich, J., Cayol, V., Okubo, P.G., 2000. The use of earthquake rate changes as a stress meter at Kilauea volcano. *Nature* 408, 457-460. <https://doi.org/10.1038/35044054>.
- Earthquake Research Committee, 2010. Prediction methods of Izu eastern seis-mic activity. The Headquarters for Earthquake Research Promotion, Ministry of Education, Culture and Sport, Science and Technology (MEXT), Japan (in Japanese). <http://www.jishin.go.jp/main/yosoku/izu/index.htm>.
- Einarsson, P., Brandsdottir, B., 1980. Seismological evidence for lateral magma intrusion during the July 1978 deflation of the Krafla volcano in NE Iceland. *Journal of Geophysics* 47(1), 160-165. <https://journal.geophysicsjournal.com/JofG/article/view/134>.
- Feuillet, N., Nostro, C., Chiarabba, C., Cocco, M., 2004. Coupling between earthquake swarms and volcanic unrest at the Alban Hills Volcano (central Italy) modeled through elastic stress transfer. *Journal of Geophysical Research* 109, B02308. <https://doi.org/10.1029/2003JB002419>.
- Geospatial Information Authority of Japan, 2016. Crustal movements in the Izu peninsula and its vicinity. Report of the Coordinating Committee for Earthquake Prediction, Japan 96, 144-163 (in Japanese). https://cais.gsi.go.jp/YOCHIREN/report/kaihou96/05_01.pdf.
- Green, D.N., Neuberg, J., 2006. Waveform classification of volcanic low-frequency earthquake swarms and its implication at Soufrière Hills Volcano, Montserrat. *Journal of Volcanology and Geothermal Research* 153(1-2), 51-63. <https://doi.org/10.1016/j.jvolgeores.2005.08.003>.
- Gutenberg, B., Richter, C.F. 1944. Frequency of earthquakes in California. *Bulletin of the Seismological Society of America* 34(4), 185-188. <https://doi.org/10.1785/BSSA0340040185>.
- Hainzl, S., Ogata, Y., 2005. Detecting fluid signals in seismicity data through statistical earthquake modeling. *Journal of Geophysical Research* 110(B5), B05S07. <https://doi.org/10.1029/2004JB003247>.
- Hayashi, Y., Morita, Y., 2003. An image of a magma intrusion process inferred from precise hypocentral migrations of the earthquake swarm east off the Izu Peninsula. *Geophysical Journal International* 153(1), 159-174. <https://doi.org/10.1046/j.1365-246X.2003.01892.x>.

- Hill, D.P., 1977. A model for earthquake swarms. *Journal of Geophysical Research* 82(8), 1347-1352.
<https://doi.org/10.1029/JB082i008p01347>.
- Ishida, M., 1984. Spatial-temporal variation of seismicity and spectrum of the 1980 earthquake swarm near the Izu Peninsula, Japan. *Bulletin of the Seismological Society of America* 74(1), 199-221.
<https://doi.org/10.1785/BSSA0740010199>.
- Kato, A., Obara, K., Igarashi, T., Tsuruoka, H., Nakagawa, S., Hirata, N., 2012. Propagation of slow slip leading up to the 2011 Mw 9.0 Tohoku-Oki earthquake. *Science* 335, 705-708.
<https://doi.org/10.1126/science.1215141>.
- Koyama, M., 1999. Pre-20th century of earthquake swarms and volcanic activity in the Higashi Izu monogenetic volcano field, based on historical documents. *The Quaternary Research (Daiyonki-Kenkyu)* 38(6), 435-446 (in Japanese with English abstract).
<https://doi.org/10.4116/jaqua.38.435>.
- Koyama, M., Umino, S., 1991. Why does the Higashi-Izu monogenetic volcano group exist in the Izu Peninsula? Relationships between late Quaternary volcanism and tectonics in the northern tip of the Izu-Bonin arc. *Journal of Physics of the Earth* 39(1), 391-420.
<https://doi.org/10.4294/jpe1952.39.391>.
- Kumazawa, T., Ogata, Y., 2013. Quantitative description of induced seismic activity before and after the 2011 Tohoku-Oki Earthquake by non-stationary ETAS models. *Journal of Geophysical Research* 118, 6165-6182. <https://doi.org/10.1002/2013JB010259>.
- Kumazawa, T., Ogata, Y., Kimura, K., Maeda, K., Kobayashi, A., 2016. Background rates of swarm earthquakes that are synchronized with volumetric strain changes. *Earth and Planetary Science Letters* 442, 51-60. <https://doi.org/10.1016/j.epsl.2016.02.049>.
- Kumazawa, T., Ogata, Y., Toda, S., 2010. Precursory seismic anomalies and transient crustal deformation prior to the 2008 Mw = 6.9 Iwate-Miyagi Nairiku, Japan, earthquake. *Journal of Geophysical Research* 115, B10312. <https://doi.org/10.1029/2010JB007567>.
- Kumazawa, T., Ogata, Y., Tsuruoka, H., 2017. Measuring seismicity diversity and anomalies by point process models: case studies before and after the 2016 Kumamoto Earthquakes in Kyushu, Japan. *Earth, Planets and Space* 69, 169. <https://doi.org/10.1186/s40623-017-0756-6>.

- Kumazawa, T., Ogata, Y., Tsuruoka, H., 2019. Characteristics of seismic activity before and after the 2018 M6.7 Hokkaido Eastern Iwate earthquake. *Earth, Planets and Space* 71, 130.
<https://doi.org/10.1186/s40623-019-1102-y>.
- Kurihara, R., Obara, K. 2021. Spatiotemporal characteristics of relocated deep low-frequency earthquakes beneath 52 volcanic regions in Japan over an analysis period of 14 years and 9 months. *Journal of Geophysical Research* 126(10), e2021JB022173.
<https://doi.org/10.1029/2021JB022173>.
- Lamb, O.D., De Angelis, S., Umakoshi, K., Hornby, A.J., Kendrick, J.E., Lavallée, Y., 2015. Repetitive fracturing during spine extrusion at Unzen volcano, Japan. *Solid Earth* 6, 1,277-1,293.
<https://doi.org/10.5194/se-6-1277-2015>.
- Lei, X., Yu, G., Ma, S., Wen, X., Wang, Q., 2008. Earthquakes induced by water injection at ~3 km depth within the Rongchang gas field, Chongqing, China. *Journal of Geophysical Research* 113(B10), B10310. <https://doi.org/10.1029/2008JB005604>.
- Llenos, A.L., McGuire, J.J., 2011. Detecting aseismic strain transients from seismicity data. *Journal of Geophysical Research* 116, B06305. <https://doi.org/10.1029/2010JB007537>.
- Llenos, A.L., McGuire, J.J., Ogata, Y., 2009. Modeling seismic swarms triggered by aseismic transients. *Earth and Planetary Science Letters* 281(1-2), 59-69.
<https://doi.org/10.1016/j.epsl.2009.02.011>.
- Miyamura, J., Ueno, H., Yokota, T., 2010. Estimation of amount of intrusive magma by using volumetric strain data and attempt of evaluation of volcanic activity in Izu-Tobu volcanoes. *Geophysical bulletin of Hokkaido University* 73, 239-255. <http://doi.org/10.14943/gbhu.73.239>.
- Morita, Y., Nakao, S., Hayashi, Y., 2006. A quantitative approach to the dike intrusion process inferred from a joint analysis of geodetic and seismological data for the 1998 earthquake swarm off the east coast of Izu Peninsula. *Journal of Geophysical Research* 111, B06208.
<https://doi.org/10.1029/2005JB003860>.
- Muramatsu, H., Takamatsu, N., Abe, S., Furuya T., Kato C., Ohno, K., Hatanaka, Y., Kakiage, Y., Ohashi, K., 2021. Updating daily solution of CORS in Japan using new GEONET 5th analysis strategy. *Journal of the Geospatial Information Authority of Japan* 134, 19-32 (in Japanese).
https://doi.org/10.57499/JOURNAL_134_03.

- Nagamune, T., Yokoyama, H., Fukudome, A., 1992. Earthquake swarms off the east coast of the Izu peninsula and their relation to the 1989 eruption of Teishi Knoll volcano. *Kazan (Bulletin of the volcanological Society of Japan)* 37(1), 1-8 (in Japanese with English abstract).
https://doi.org/10.18940/kazan.37.1_1.
- Nanjo, K.Z., 2020. Were changes in stress state responsible for the 2019 Ridgecrest, California, earthquakes? *Nature Communications* 11, 3082. <https://doi.org/10.1038/s41467-020-16867-5>.
- Nanjo, K.Z., Yoshida, A. 2018. A *b* map implying the first eastern rupture of the Nankai Trough earthquakes. *Nature Communications* 9(1), 1117. <https://doi.org/10.1038/s41467-018-03514-3>.
- Nanjo, K.Z., Yukutake, Y., Kumazawa, T., 2023. Activated volcanism of Mount Fuji by the 2011 Japanese large earthquakes. *Scientific Reports* 13, 10562.
<https://doi.org/10.1038/s41598-023-37735-4>.
- Obara, K., 2002. Nonvolcanic deep tremor associated with subduction in southwest Japan. *Science* 296(5573), 1,679-1,681. <https://doi.org/10.1126/science.1070378>.
- Ogata, Y., 1988. Statistical models for earthquake occurrences and residual analysis for point processes. *Journal of the American Statistical Association* 83, 9-27.
<https://doi.org/10.2307/2288914>.
- Ogata, Y., 1992. Detection of precursory relative quiescence before great earthquakes through a statistical model. *Journal of Geophysical Research* 97, 19,845-19,871.
<https://doi.org/10.1029/92JB00708>.
- Ogata, Y., 2006. *Statistical Analysis of Seismicity-updated version (SASeis2006)*. ISM Computer Science Monographs, No. 33, The Institute of Statistical Mathematics, Tokyo, Japan.
https://www.ism.ac.jp/~ogata/Ssg/ssg_softwaresE.html (manual and codes).
- Ogata, Y., Tsuruoka, H., 2016. Statistical monitoring of aftershock sequences: a case study of the 2015 Mw7.8 Gorkha, Nepal, earthquake. *Earth, Planets and Space* 68, 44.
<https://doi.org/10.1186/s40623-016-0410-8>.
- Okada, Y., Yamamoto, E., 1991. Dyke intrusion model for the 1989 seismovolcanic activity off Ito, Central Japan. *Journal of Geophysical Research* 96(B6), 10,361-10,376.
<https://doi.org/10.1029/91JB00427>.

- Okada, Y., Yamamoto, E., Ohkubo T., 2000. Coswarm and preswarm crustal deformation in the eastern Izu Peninsula, central Japan. *Journal of Geophysical Research* 105(B1), 681-692. <https://doi.org/10.1029/1999JB900335>.
- Ozawa, S., Miyazaki, S., Hatanaka, Y., Imakiire, T., Kaidzu, M., Murakami, M., 2003. Characteristic silent earthquakes in the eastern part of the Boso peninsula, Central Japan. *Geophysical Research Letters* 30(6), 1283. <https://doi.org/10.1029/2002GL016665>.
- Peng, Z., Zhao, P., 2009. Migration of early aftershocks following the 2004 Parkfield earthquake. *Nature Geoscience* 2, 877-881. <https://doi.org/10.1038/ngeo697>.
- Petersen, T., 2007. Swarms of repeating long-period earthquakes at Shishaldin Volcano, Alaska, 2001-2004. *Journal of Volcanology and Geothermal Research* 166(3-4), 177-192. <https://doi.org/10.1016/j.jvolgeores.2007.07.014>.
- Ross, Z.E., Idini, B., Jia, Z., Stephenson, O.L., Zhong, M., Wang, X., Zhan, Z., Simons, M., Fielding, E.J., Yun, S.-H., Hauksson, E., Moore, A.W., Liu, Z., Jung, J., 2019. Hierarchical interlocked orthogonal faulting in the 2019 Ridgecrest earthquake sequence. *Science* 366(6463), 346-351. <https://doi.org/10.1126/science.aaz0109>.
- Schorlemmer, D., Neri, G., Wiemer, S., Mostaccio, A., 2003. Stability and significance tests for *b*-value anomalies: example from the Tyrrhenian Sea. *Geophysical Research Letters* 30(16), 1835. <https://doi.org/10.1029/2003GL017335>.
- Segall, P., Desmarais, E.K., Shelly, D., Miklius, A., Cervelli, P., 2006. Earthquakes triggered by silent slip events of Kilauea volcano, Hawaii. *Nature* 442, 71-74. <https://doi.org/10.1038/nature04938>.
- Shelly, D.R., Beroza, G.C., Ide, S., 2007. Non-volcanic tremor and low-frequency earthquake swarms. *Nature* 446, 305-307. <https://doi.org/10.1038/nature05666>.
- Shimazaki, K., 1988. Dyke intrusion hypothesis at east off Izu Peninsula. Abstracts, vol. 1, p. 330, Seismological Society of Japan, Tokyo (in Japanese).
- Shishikura, M., Namegaya, Y., Kaneko, H., Koyama, M., 2023. Late Holocene tectonics inferred from emerged shoreline features in Higashi-Izu monogenetic volcano field, Central Japan. *Tectonophysics* 864, 229985. <https://doi.org/10.1016/j.tecto.2023.229985>.
- Smith, K.D., von Seggern, D., Blewitt, G., Preston, L., Anderson, J.G., Wernicke, B.P., Davis, J.L., 2004. Evidence for deep magma injection beneath Lake Tahoe, Nevada-California. *Science* 305(5688), 1277-1280. <https://doi.org/10.1126/science.1101304>.

- Tada, T., Hashimoto, M., 1989. On the cause of abnormal crustal deformation in the northeastern Izu Peninsula 3, Open crack model and activity in the summer of 1988, Abstracts, vol. 1, p. 41, Seismological Society of Japan, Tokyo (in Japanese).
- Takamatsu, N., Muramatsu, H., Abe, S., Hatanaka, Y., Furuya, T., Kakiage, Y., Ohashi, K., Kato, C., Ohno, K., Kawamoto, S., 2023. New GEONET analysis strategy at GSI: daily coordinates of over 1300 GNSS CORS in Japan throughout the last quarter century. *Earth, Planets and Space* 75, 49. <https://doi.org/10.1186/s40623-023-01787-7>.
- Terakawa, T., 2014. Evolution of pore fluid pressures in a stimulated geothermal reservoir inferred from earthquake focal mechanisms. *Geophysical Research Letters* 41(21), 7468–7476. <https://doi.org/10.1002/2014GL061908>.
- Terakawa, T., Hashimoto, C., Matsu'ura, M., 2013. Changes in seismic activity following the 2011 Tohoku-oki Earthquake: effects of pore fluid pressure. *Earth and Planetary Science Letters* 365, 17-24. <https://doi.org/10.1016/j.epsl.2013.01.017>.
- Toda, S., Stein, R., Sagiya, T., 2002. Evidence from the A.D. 2000 Izu Islands swarm that seismicity is governed by stressing rate. *Nature* 419, 58-61. <https://doi.org/10.1038/nature00997>.
- Ukawa, M., 1991. Collision and fan-shaped compressional stress pattern in the Izu block at the northern edge of the Philippine Sea plate. *Journal of Geophysical Research* 96(B1), 713-728. <https://doi.org/10.1029/90JB02142>.
- Utsu, T. 1961. A statistical study on the occurrence of aftershocks. *Geophysical Magazine* 30(4), 521-605.
- Wessel, P., Smith, W.H.F., Scharroo, R., Luis, J.F., Wobbe, F., 2013. Generic Mapping Tools: improved version released. *EOS, Transactions, AGU* 94(45), 409-410. <https://doi.org/10.1002/2013EO450001>.
- Wiemer, S., 2001. A software package to analyze seismicity: ZMAP. *Seismological Research Letters* 72(3), 373-382. <https://doi.org/10.1785/gssrl.72.3.373>.
- Waite, G.P., Smith, R.B., 2002. Seismic evidence for fluid migration accompanying subsidence of the Yellowstone caldera. *Journal of Geophysical Research* 107(B9), 2177. <https://doi.org/10.1029/2001JB000586>.

- Woessner, J., Wiemer, S., 2005. Assessing the quality of earthquake catalogues: estimating the magnitude of completeness and its uncertainty. *Bulletin of the Seismological Society of America* 95, 684-698. <https://doi.org/10.1785/0120040007>.
- Yamamoto, T., Soya, T., Suto, S., Uto, K., Takada, A., Sakaguchi, K., Ono, K., 1991. The 1989 submarine eruption off eastern Izu Peninsula, Japan: ejecta and eruption mechanisms. *Bulletin of Volcanology* 53, 301-308. <https://doi.org/10.1007/BF00414526>.
- Yukutake, Y., 2017. Development of a routine system for a deep-low frequency earthquake in Hakone Volcano, by using the matched filter method. *Bulletin of the Hot Springs Research Institute of Kanagawa Prefecture* 49, 1-10 (in Japanese with English abstract). https://www.onken.odawara.kanagawa.jp/files/PDF/houkoku/49/houkoku49_p01-10.pdf.
- Yukutake, Y., Abe, Y., Doke, R. 2019. Deep low-frequency earthquakes beneath the Hakone volcano, central Japan, and their relation to volcanic activity. *Geophysical Research Letters* 46(20), 11,035-11,043. <https://doi.org/10.1029/2019GL084357>.

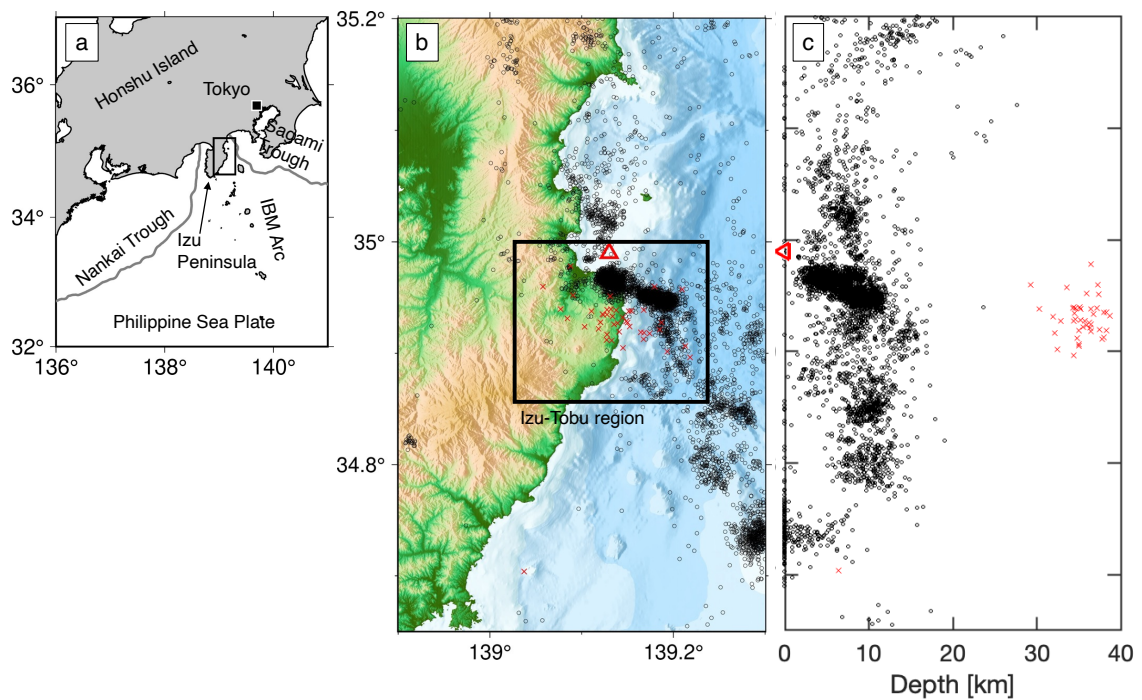


Fig. 1| Seismicity in and around the study region. **a**, Central Japan including the region (black rectangle) of **b**. Gray curves indicate trough axes. IBM Arc: Izu-Bonin-Mariana Arc. **b**, Map showing ordinary earthquakes with $M \geq 1$ (black circle) and LFEs with $M \geq 0.1$ (red cross) at depths 0-40 km during the period Jan. 2005-Dec. 2020. To plot these earthquakes, the JMA catalog was used. Red triangle indicates the Teishi Knoll. Black rectangle indicates the study region called the Izu-Tobu region. **c**, Cross-sectional view of ordinary earthquakes and LFEs.

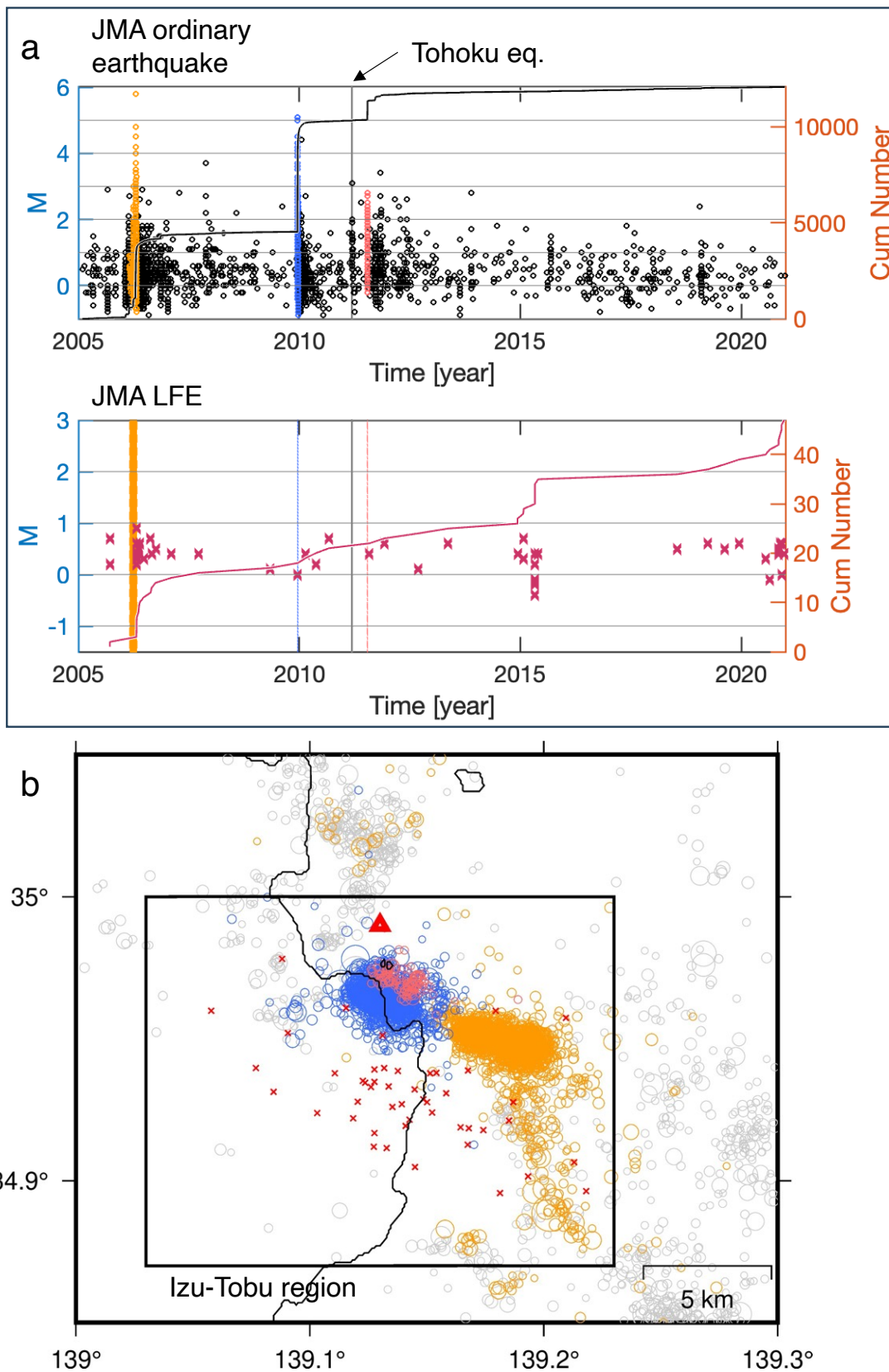


Fig. 2| Space-time distribution of earthquakes in the Izu-Tobu region. a, Top panel: M -time diagram (y-axis on the left side) of ordinary earthquakes (depths of 0-40 km) in the study region

indicated by a black rectangle in **b**. These earthquakes were obtained from the JMA catalog. Overlapped is the cumulative number of ordinary earthquakes as a function of time (y-axis on the right side). Three abrupt increases of the cumulative number of ordinary earthquakes indicate three earthquake swarms. Based on GSI (2016), earthquakes in the periods Mar. 1-Apr. 30, 2006 (orange), Dec. 17-21, 2009 (blue), and Jul. 17-18, 2011 (pink) were considered as the 2006, 2009, and 2011 swarms, respectively. Vertical line indicates the moment of the Mar. 11, 2011 M_9 Tohoku earthquake. Bottom panel: same as the top panel for LFEs. Orange, blue, and pink vertical lines indicate the 2006, 2009, and 2011 swarms, respectively. **b**, Map showing ordinary earthquakes (circle) and LFEs (cross) in and around the study region (black rectangle). Earthquakes with $M \geq 1$ (depths of 0-40 km) in orange, blue, and pink, are the 2006, 2009, and 2011 swarms, respectively. Other ordinary earthquakes are indicated by grey circles. Triangle indicates the Teishi Knoll.

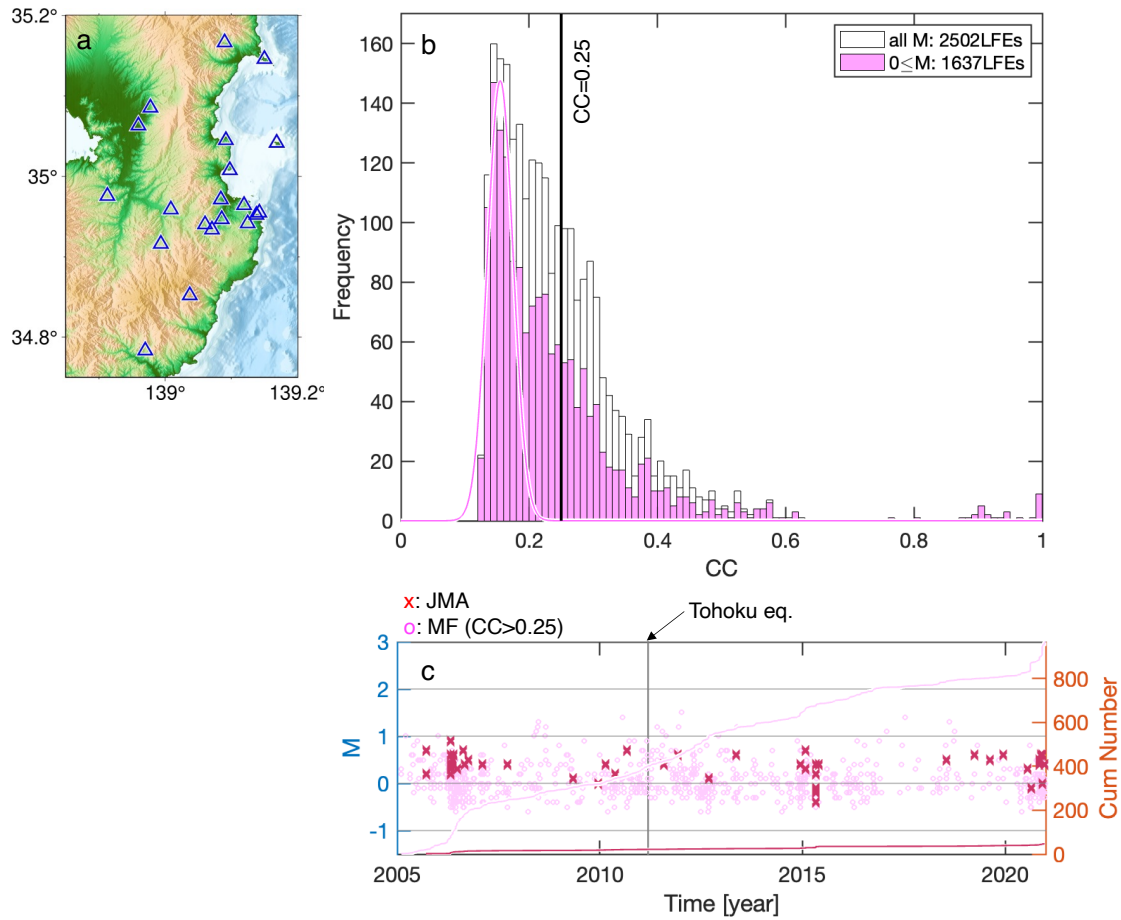


Fig. 3 | LFEs detected by the MF method. **a**, Stations that recorded waveforms used in this study. **b**, Multiple histograms of CC -values for all magnitudes (white) and $M \geq 0$ (pink). Also included is the normally distributed curve (mean of 0.155 and standard deviation of 0.02). Vertical line indicates $CC = 0.25$. **c**, Same as the bottom panel of Fig. 2a, but data from the MF catalog ($CC > 0.25$) are included, as shown in pink. Vertical line indicates the moment of the 2011 Tohoku earthquake.

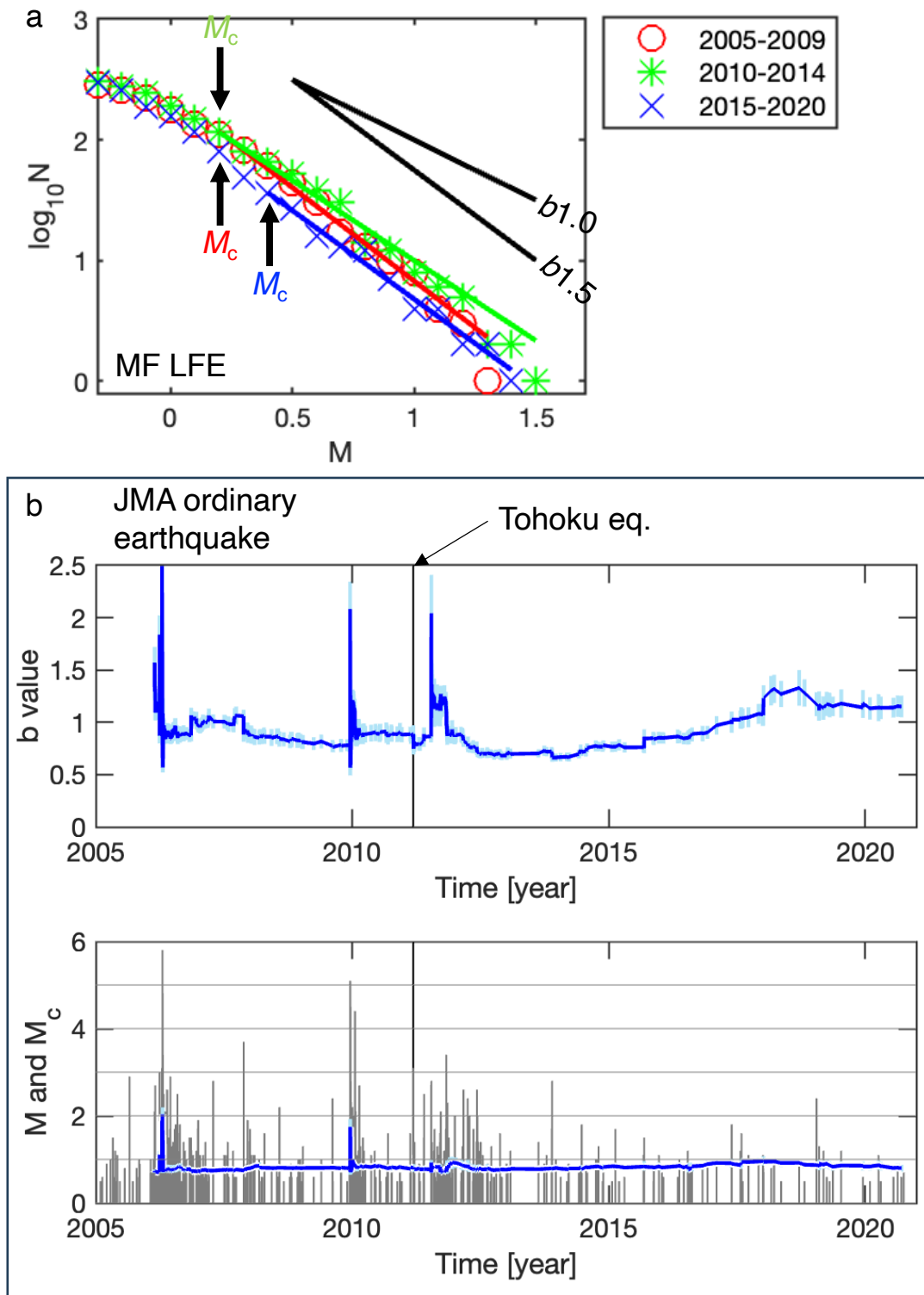


Fig. 4| M_c of LFEs and ordinary earthquakes. **a**, The MF catalog ($CC > 0.25$) was used. (**b**, a , M_c) = (1.55 ± 0.10, 2.38, 0.2) for 2005-2009, (1.33 ± 0.10, 2.33, 0.2) for 2010-2014, and (1.47 ± 0.20, 2.15, 0.4) for 2015-2020. **b**, JMA catalog was used. Top panel: b -value as a function of time. Bottom panel: M and M_c as a function of time. Vertical line indicates the moment of the Tohoku earthquake.

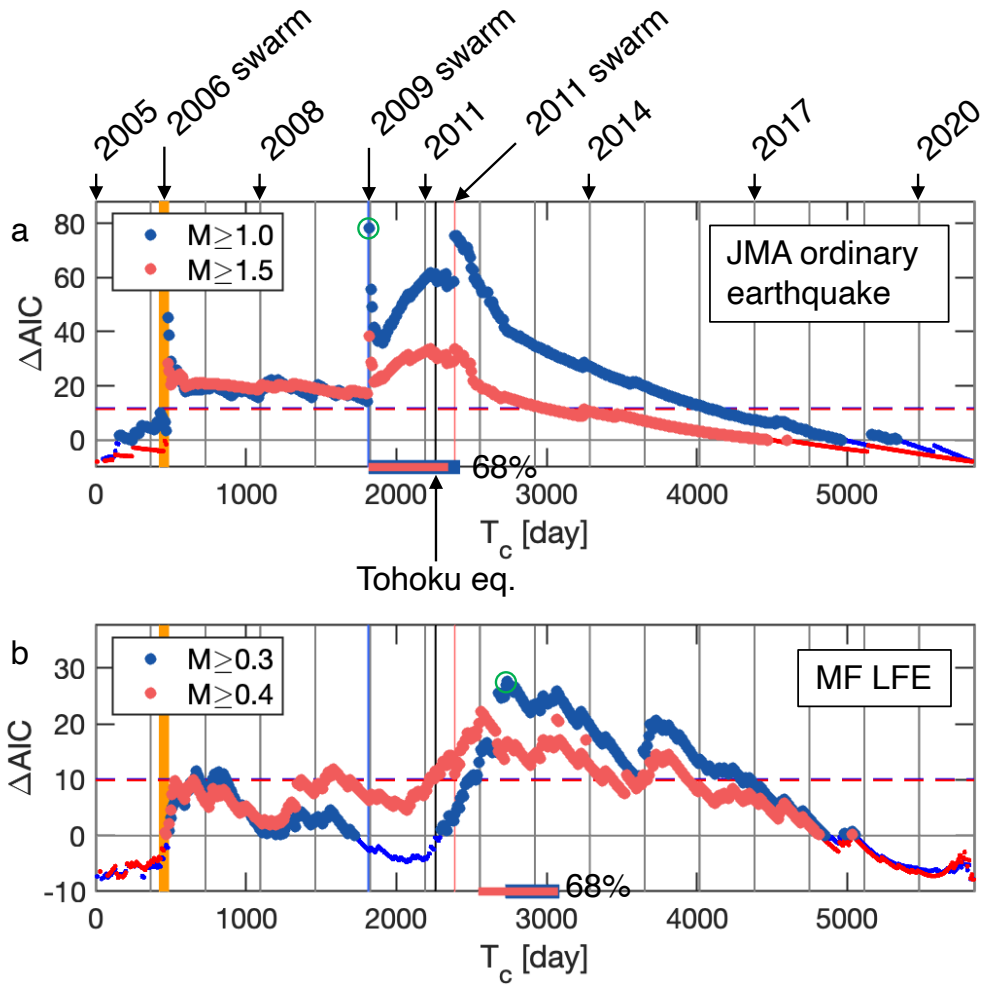


Fig. 5| First-order timeseries analysis. a, $\Delta AIC = AIC_{\text{single}} - AIC_{\text{2stage}}$ as a function of T_c is shown taking $M_{th}=1.0$ (blue data) and $M_{th}=1.5$ (red data) from the JMA catalog of ordinary earthquakes. Small points show that the model-fitting analysis did not converge when assuming the corresponding T_c . As a reference, grey vertical lines indicate Jan. 1 for 2004–2019. The timing of the Tohoku earthquake is shown by a black vertical line. Orange, blue, and red vertical lines indicate the moment of 2006, 2009, 2011 swarms, respectively. Horizontal dashed lines representing $2q$ for $M_{th}=1.0$ (blue) and $M_{th}=1.5$ (red) overlap, where q is the degree of freedom imposed when searching T_c based on the data over the entire period. The blue horizontal bars represent the change points' confidence intervals of 68% (top bar) for $M_{th}=1.0$. The red horizontal bars are the same as the blues ones for $M_{th}=1.5$. The ETAS fitting for the data point indicated by a green circle is shown in Fig. 6. b, Same as a for the MF catalog ($CC > 0.25$) of LFEs with $M_{th}=0.3$ (blue) and $M_{th}=0.4$ (red).

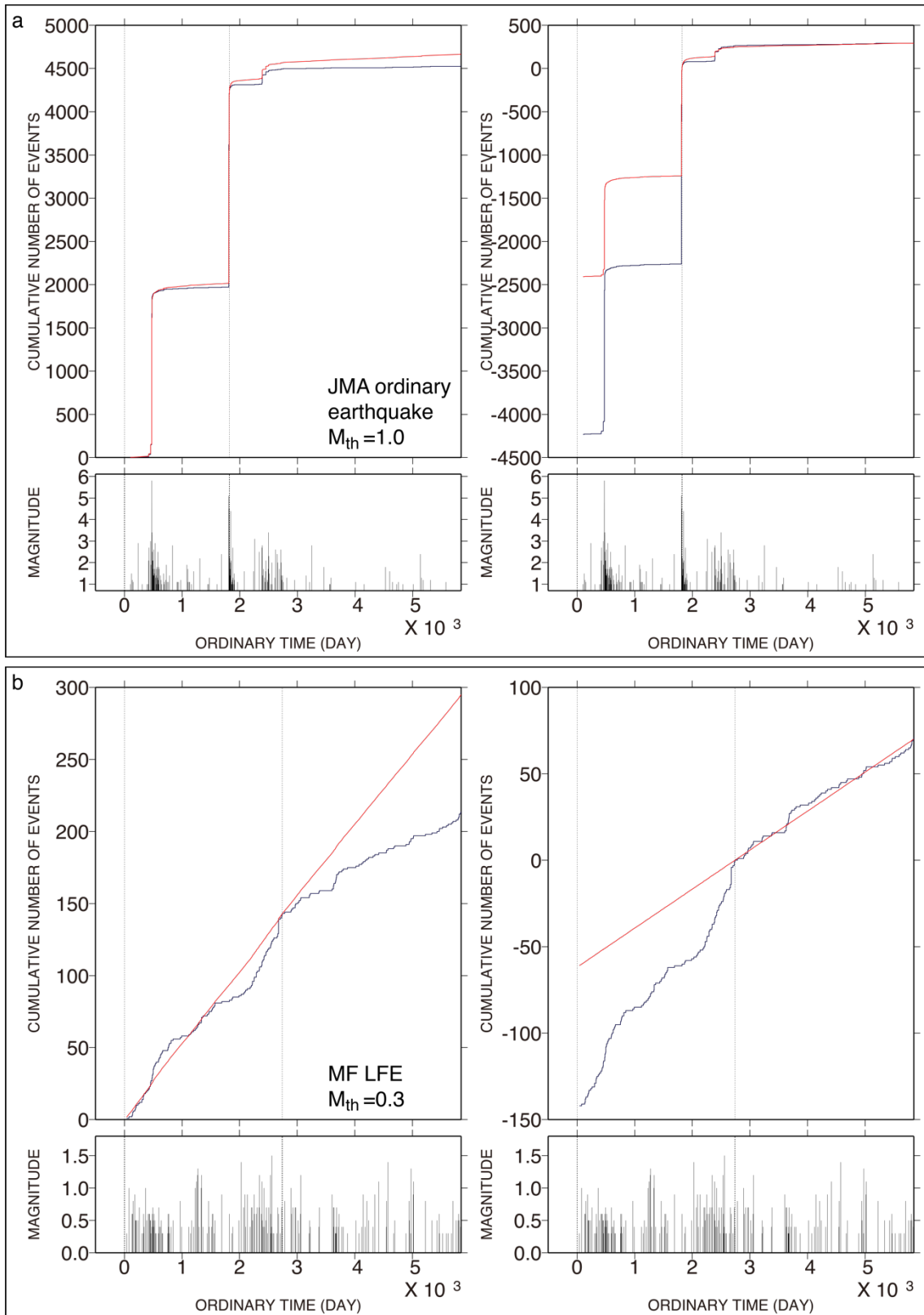


Fig. 6| Change point analysis for the first-order timeseries analysis. **a**, Left panel: Cumulative function of $M \geq 1.0$ for ordinary earthquakes (black curve) is plotted against ordinary time, showing the

ETAS fitting (red curve) in the target interval from Jan. 2005 (first vertical line) until immediately before $T_c=1820$ days (second vertical line) (green circle in Fig. 5a), and then extrapolated until Dec. 2020. Right panel: As in the left panel except that the target is the later time interval after $T_c=1820$ days. Below these panels, the same M -time diagram is shown. $\theta=(\mu, K_0, c, \alpha, p)=(0.019, 0.032, 0.001, 0.058, 1.40)$ for the left panel and $(0.003, 0.024, 0.001, 0.000, 1.27)$ for the right panel. **b**, As in **a** except for LFEs ($M \geq 0.3$) and $T_c=2740$ days (green circle in Fig. 5b). $\theta=(0.046, 0.00035, 0.001, 0.00, 1.80)$ for the left panel and $(0.023, 0.00000, 0.001, 0.00, 1.58)$ for the right panel.

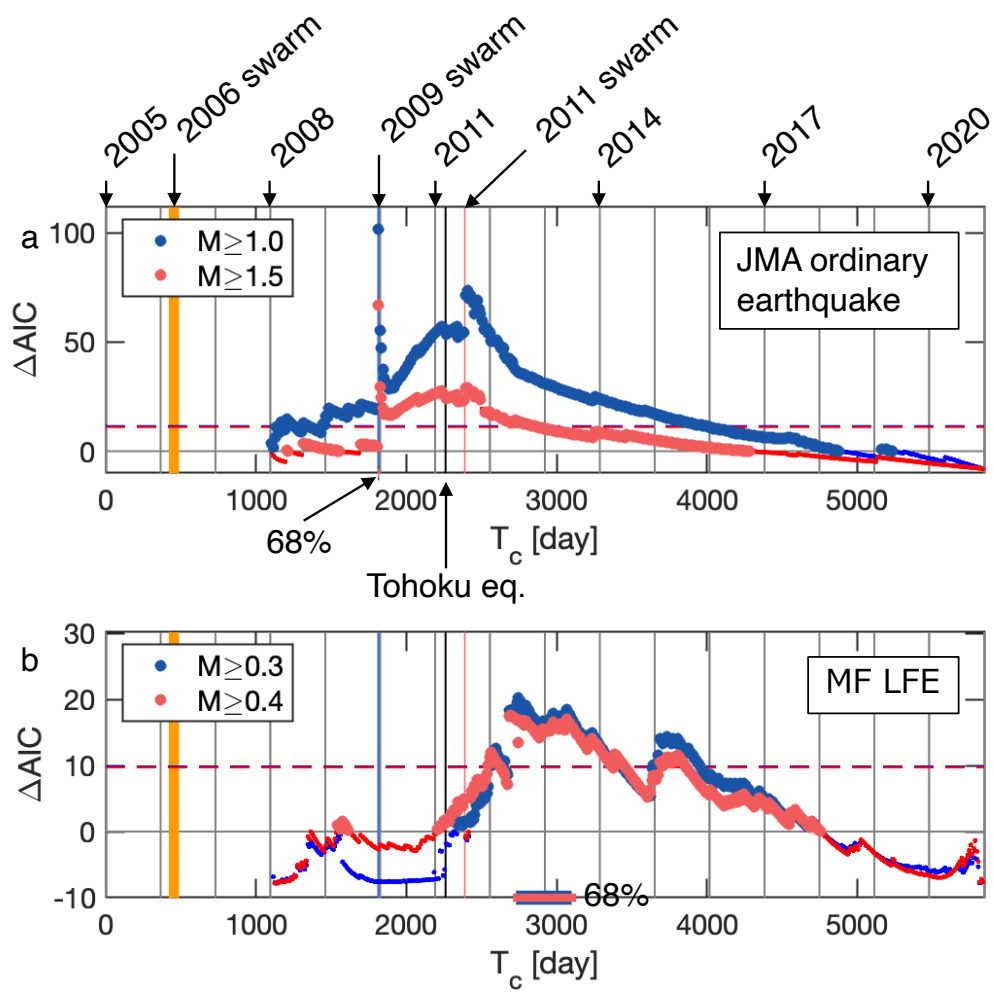


Fig. 7 | Same as Fig. 5 for seismicity since Jan. 2008.

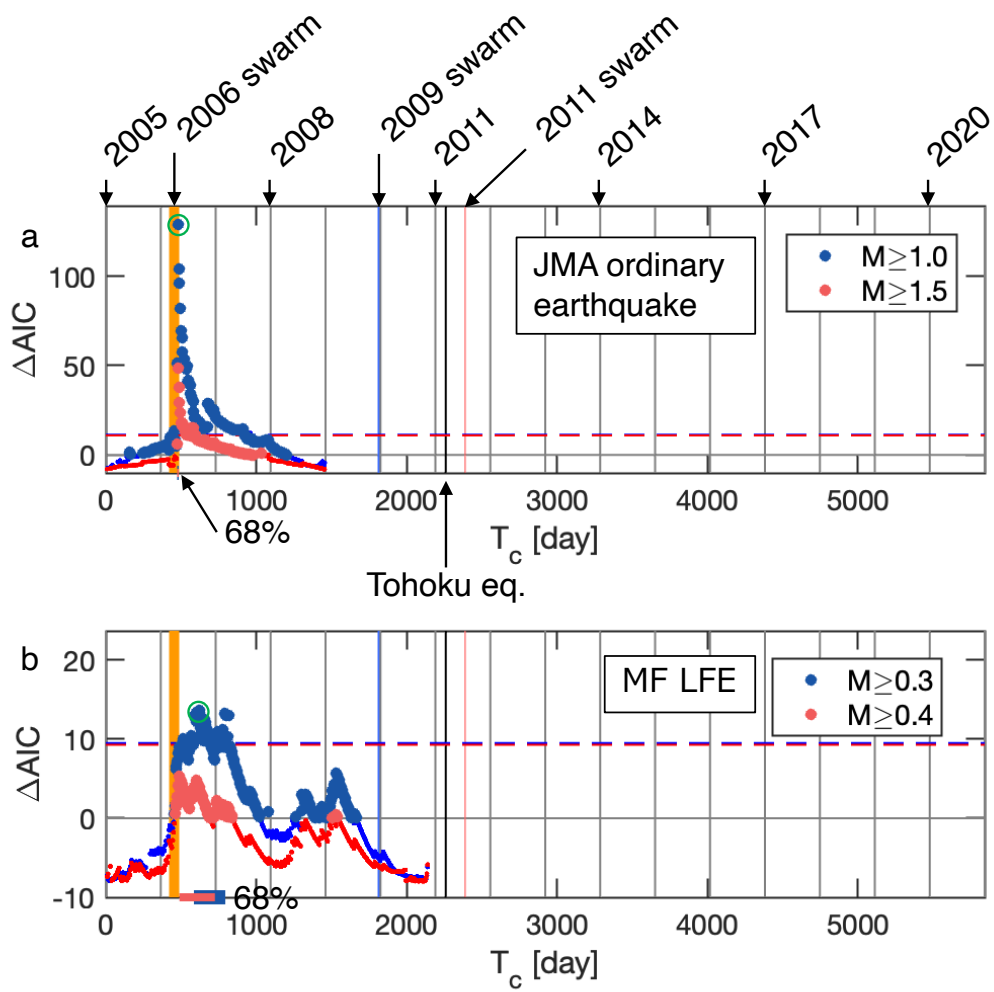


Fig. 8| Same as Fig. 5 for the second-order timeseries analysis.

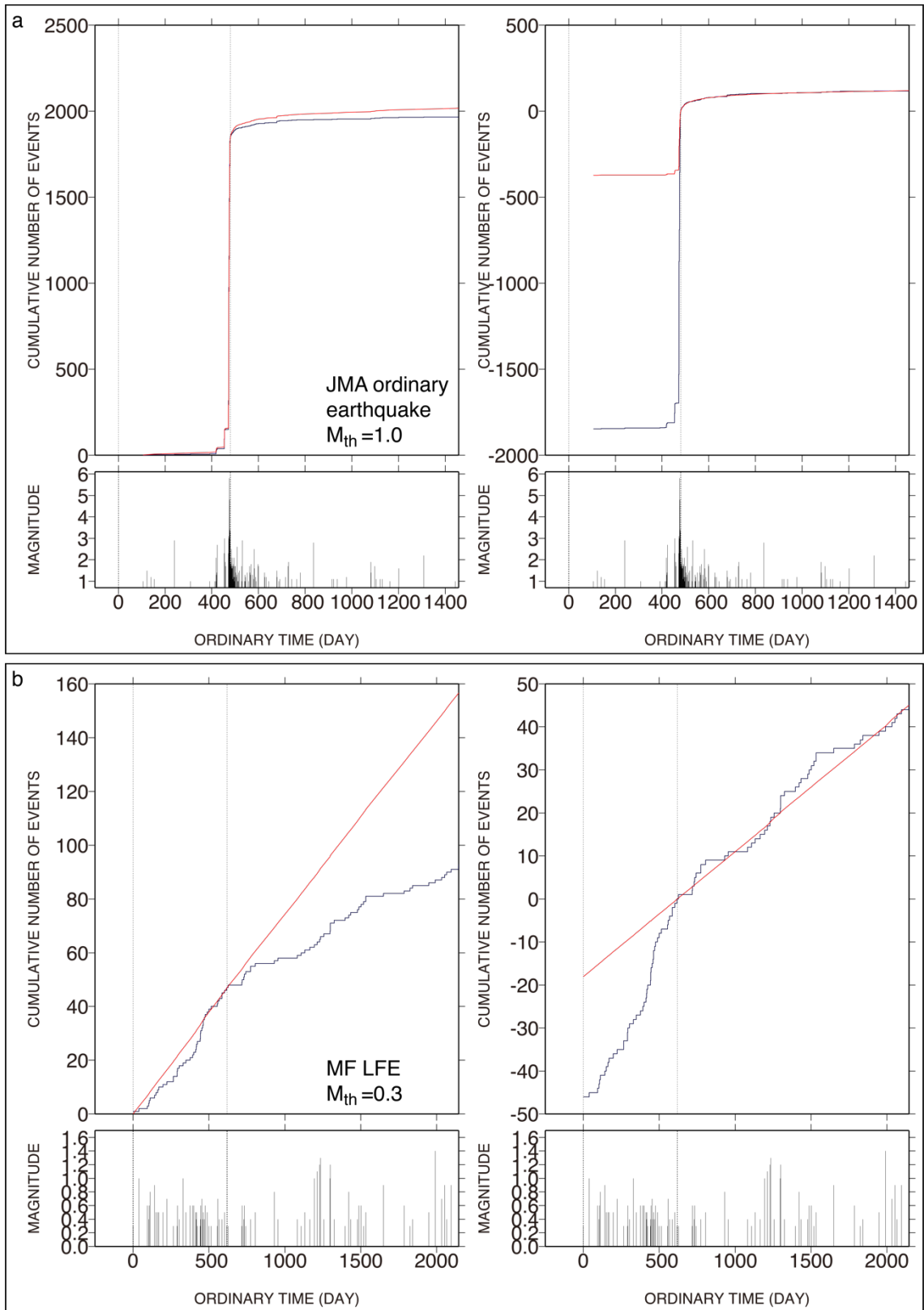


Fig. 9| Same as Fig. 6 for second-order timeseries analysis. a, Left panel: Cumulative function of $M \geq 1.0$ for ordinary earthquakes (black curve) is plotted against ordinary time, showing the ETAS

fitting (red curve) in the target interval from Jan. 2005 (first vertical dashed line) until immediately before $T_c=480$ days (second vertical dashed line) (green circle in Fig. 8a), and then extrapolated until Dec. 2008. Right panel: As in the left panel except that the target is the later time interval after $T_c=480$ days. $\theta=(\mu, K_0, c, \alpha, p)=(0.024, 0.03, 0.001, 0.14, 1.47)$ for the left panel and $(0.010, 0.07, 0.001, 0.34, 1.12)$ for the right panel. **b**, As in **a** except for LFEs with $M \geq 0.3$. The ETAS model was fitted to the target interval from Jan. 2005 until immediately before $T_c=620$ days (green circle in Fig. 8b), and then extrapolated until Dec. 2010. $\theta=(0.069, 0.00014, 0.001, 0.00, 1.91)$ for the left panel and $(0.029, 0.00000, 0.001, 5.69, 4.51)$ for the right panel.

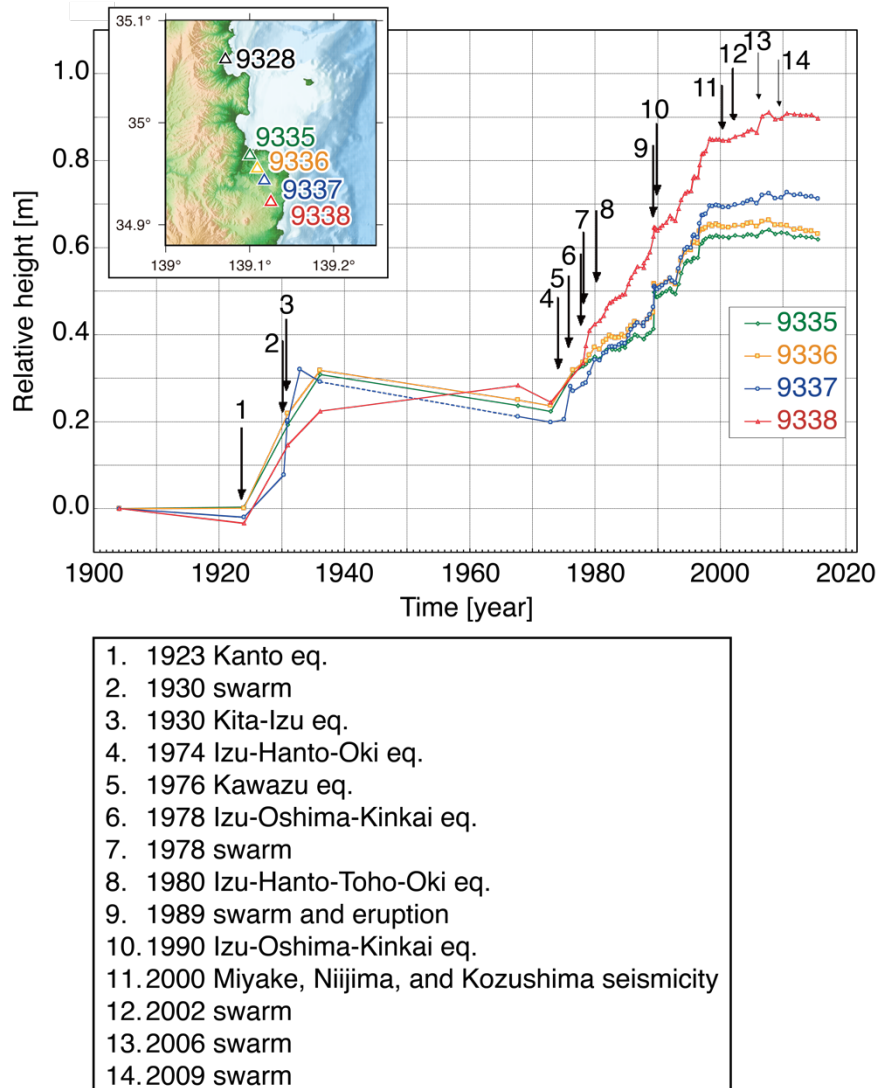


Fig. 10| Timeseries of vertical crustal movement. The leveling survey refers to benchmark 9328. Taking the year 1904 as the reference time, the results were obtained by the leveling survey at benchmarks 9335, 9336, 9337, and 9338, whose locations are mapped in the inset. Data points and arrows in the figure were reproduced from GSI (2016). Inset shows the locations of the benchmarks.

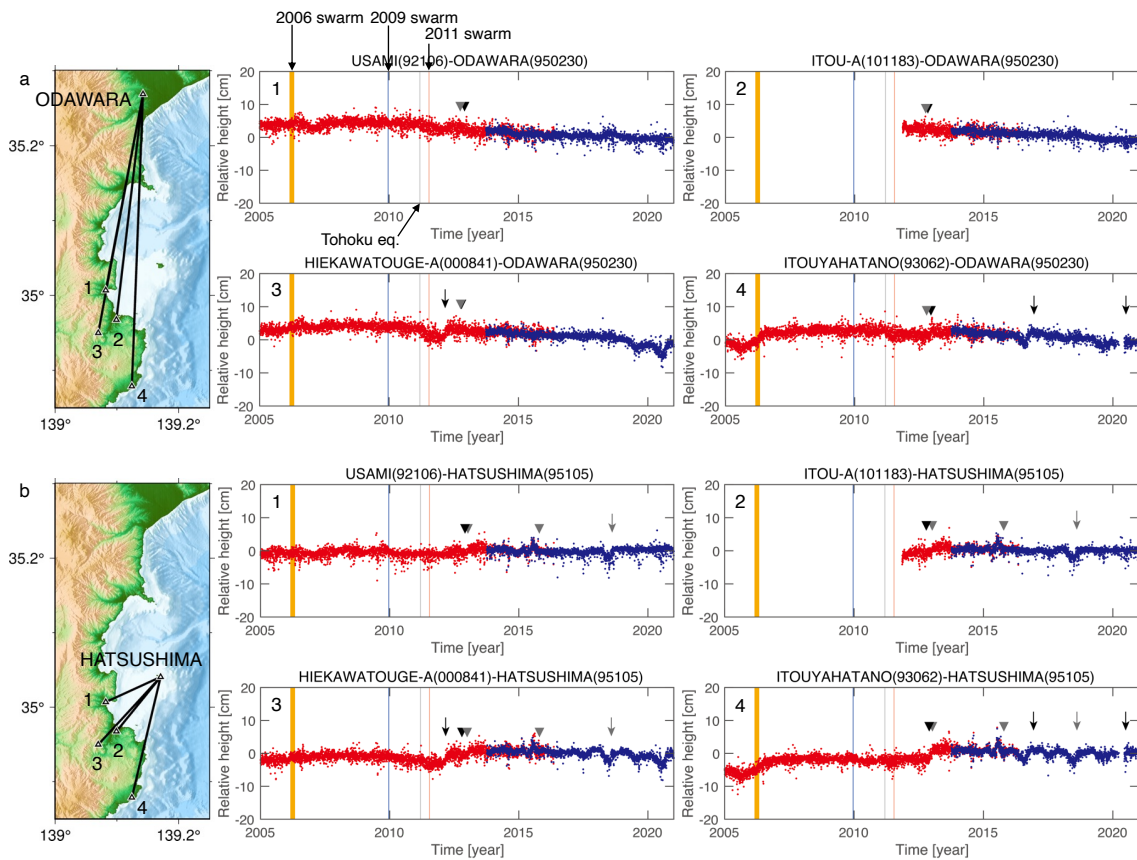


Fig. 11| Baseline changes. **a**, left panel: map showing stations (triangle) and baselines (segment). Reference station is ODAWARA, and stations 1, 2, 3, and 4 are USAMI, ITOU-A, HIEKAWATOUGE, and ITOUYAHATANO-A, respectively. Middle top panel: relative heights of station 1 (USAMI) to the reference station (ODAWARA) as a function of time. Red and blue dots are F3 and F5 solutions, respectively. Grey vertical line indicates the moment of the Tohoku earthquake. Orange, blue, and pink vertical lines indicate the moment of 2006, 2009, 2011 swarms, respectively. Right top panel: same as the middle top panel for ITOU-A. Middle bottom panel: same as the middle top panel for HIEKAWATOUGE. Right bottom panel: same as the middle top panel for ITOUYAHATANO-A. **b**, Same as **a** for reference station HATSUSHIMA. Major maintenance: triangle indicates antenna replacement of stations 1-4 (black) and the reference station (grey), and arrow indicates tree trimming around stations 1-4 (black) and the reference station (grey).

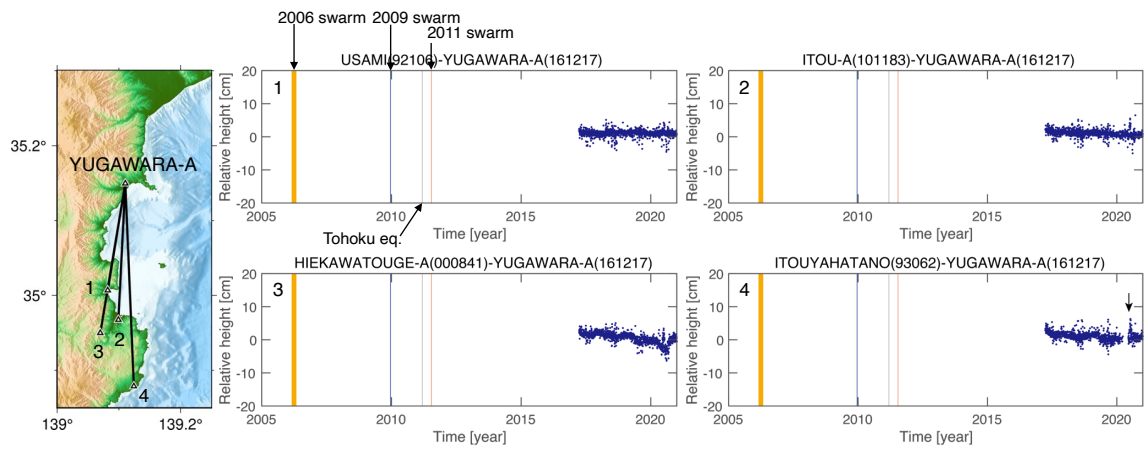


Fig. 12| Same as Fig. 11 for reference station YUGAWARA-A.